Taylor & Francis
Taylor & Francis Group

Check for updates

Adsorption of methyl orange on low-cost adsorbent natural materials and modified natural materials: a review

Muna Abd Ul Rasool AL-Kazragi[a], Dhafir T. A. AL-Heetimi[a] (iD), and Lee D. Wilson[b] (iD)

[a]Department of Chemistry, College of Education for Pure Science Ibn-Al-Haitham, University of Baghdad, Baghdad, Iraq; [b]Department of Chemistry, College of Art and Science, University of Saskatchewan, Saskatoon, Canada

ABSTRACT

Recently a large number of extensive studies have amassed that describe the removal of dyes from water and wastewater using natural adsorbents and modified materials. Methyl orange dye is found in wastewater streams from various industries that include textiles, plastics, printing and paper among other sources. This article reviews methyl orange adsorption onto natural and modified materials. Despite many techniques available, adsorption stands out for efficient water and wastewater treatment for its ease of operation, flexibility and large-scale removal of colorants. It also has a significant potential for regeneration recovery and recycling of adsorbents in comparison to other water treatment methods. The adsorbents described herein were classified into five categories based on their chemical composition: bio-sorbents, activated carbon, biochar, clays and minerals, and composites. In this review article, we want to demonstrate the capacity of natural and modified materials for dye adsorption which can yield significant improvements to the adsorption capacity of dyes such as methyl orange. In addition, the effect of critical variables including contact time, initial methyl orange concentration, dosage of adsorbent, pH, temperature and mechanism on the adsorption efficiency will be covered as part of this literature review.

NOVELTY STATEMENT

- The novelty of this review article describes the utility of various natural and modified materials employed to remove methyl orange (MO) from water, wastewater and aqueous solutions. Natural sorbents are very popular adsorbents because the majority of them are affordable and readily accessible in terms of addressing key challenges concerning water security that are relevant to MO adsorption processes.
- This review is significant since it will be useful in guiding researchers on the selection of an adsorbent that would be suitable for MO adsorption. Furthermore, our findings provide a basis for researchers interested in the design of composite adsorbents based on the selection of constituent components.

Introduction

Water pollution is a serious issue since it has become increasingly serious with particular reference to dye species. According to the WHO and UNICEF in a 2000 report, approximately 70–80% of total illnesses in developing countries are caused by different water contaminants that predominantly affect women and children. Water is an essential and indispensable component of our biosphere, which is critically important for the maintenance of all life forms on earth. The presence of various organic compounds, inorganics, micro-organisms, hazardous chemical wastes or industrial/domestic wastes contributes to impurities in water that make it unsuitable for human consumption purposes (Khapre et al. 2021). The estimated annual production of dyes around the world is over 700,000 tons with 10,000 kinds of color, of which 10–15% are discharged into the environment by produced wastewaters. It has been widely reported in the literature that industries mainly generate a strongly colored wastewater with a concentration in the range of 10–200 mg/L (Kermani et al. 2017). The effects of release of organic dye molecules into water result in a number of water quality impacts such as decreased dissolved oxygen and decreased penetration of sunlight, which affects photosynthesis in aquatic ecosystems (Yadav et al. 2021; Pandey et al. 2022). Rubber, paper, leather, textiles, cosmetics, and petroleum are examples of everyday industrial items that are released along with anionic azo dyes into marine environments (Su et al. 2014). Azo dyes are mainly employed as a pH indicator for titrations in analytical chemistry laboratories (Mittal et al. 2007) and are well-known chemical cancer-causing agents. MO, like most other dyes of this category are metabolized into aromatic byproducts by microbes upon ingestion by humans. Reductive enzymes in the liver are able to create aromatic amines by catalyzing the reductive dissociation of the azo bond, which may result in the onset of intestinal cancer (Su et al. 2014). After skin contact, MO is therefore classified as an allergenic substance

that might result in skin eczema (Haddadian et al. 2013). Because of the harm to human health posed by the discharge of this toxic dye into water bodies without suitable treatment, major issues can also arise because the dye's hue is readily visible in water even at low concentrations (Deligeer et al. 2011). The characteristics of dye compounds such as MO have generated some challenging environmental problems, such as increasing the chemical oxygen demand (COD) of wastewater, which reduces photosynthetic activity in aquatic environments. This can make the wastewater
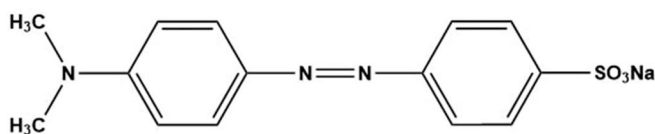

Figure 1. Molecular structure of methyl orange (MO) dye.

Table 1. Characteristics of MO.

Property	Parameter description
IUPAC name	Sodium-4-(4-dimethylamino phenyl diazenyl) benzenesulfonate
Molecular formula	$C_{14}H_{14}N_3SO_3Na$
Molecular weight	327.34 g/mol
pKa	3.4
pH	6.5 (5 g/l, H_2O, 20 °C)
pH range	3.1(Red)-4.4(Orange)
Color and form	Orange-yellow powder or crystalline scales
Melting point	>300 °C
Density	0.987 g/mL at 25 °C
Storage temp.	Store at +5 °C to +30 °C.
Solubility	Less than 1 mg/mL at 18 C

toxic and even mutagenic if degraded by anaerobic digestion. Furthermore, based on regulations for waste color, a low concentration of visible dye is intolerable that can cause hazards toward human health (Haddadian et al. 2013). MO is a representative contaminant in industrial wastewater with poor biodegradability (Krika and Benlahbib 2015). Figure 1 and Table 1 describe the chemical composition and physico-chemical characteristics of MO. According to the origin, carcinogenicity, presence of arene rings in the dye structure, the water solubility and mode of application of such dyes (particularly anionic dyes) are categorized as shown in Figure 2.

As a result, it is required to remove weak acid dyes such as MO from aqueous media. The great chemical and thermal stability of this anionic dye causes certain challenges in its removal from water and wastewater (Bhatnagar and Sillanpää 2010). Figure 3 lists various chemical, physical, and biological techniques along with their benefits and drawbacks. There are many techniques, such as: electrochemical (Bechtold et al. 2001; Pandey et al. 2022), chemical coagulation/flocculation (Papić et al. 2004; Agbovi and Wilson 2021), photo-catalytic degradation using UV/TiO$_2$ (Sohrabi and Ghavami 2008), electrochemical precipitation (Fan 2008) are employed for dye removal. However, most of these methods have certain drawbacks, such as the operational and capital costs, which are considered to be the major limiting factors when applying these methods. In addition, there are handling costs related to sludge production and disposal of hazardous by-products; (Kalantry et al. 2016; Jafari et al. 2016) whereas the adsorption process which is regarded one of preferred physico–chemical treatment
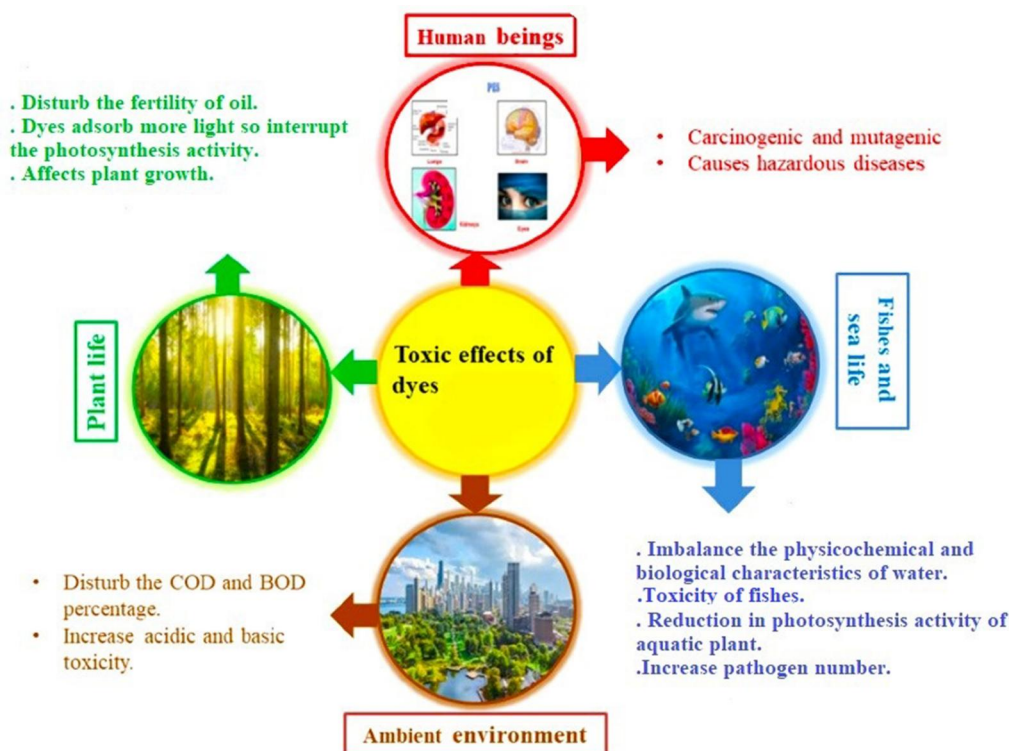

Figure 2. Toxic effects of dyes on environment and living beings (Yadav et al. 2021).
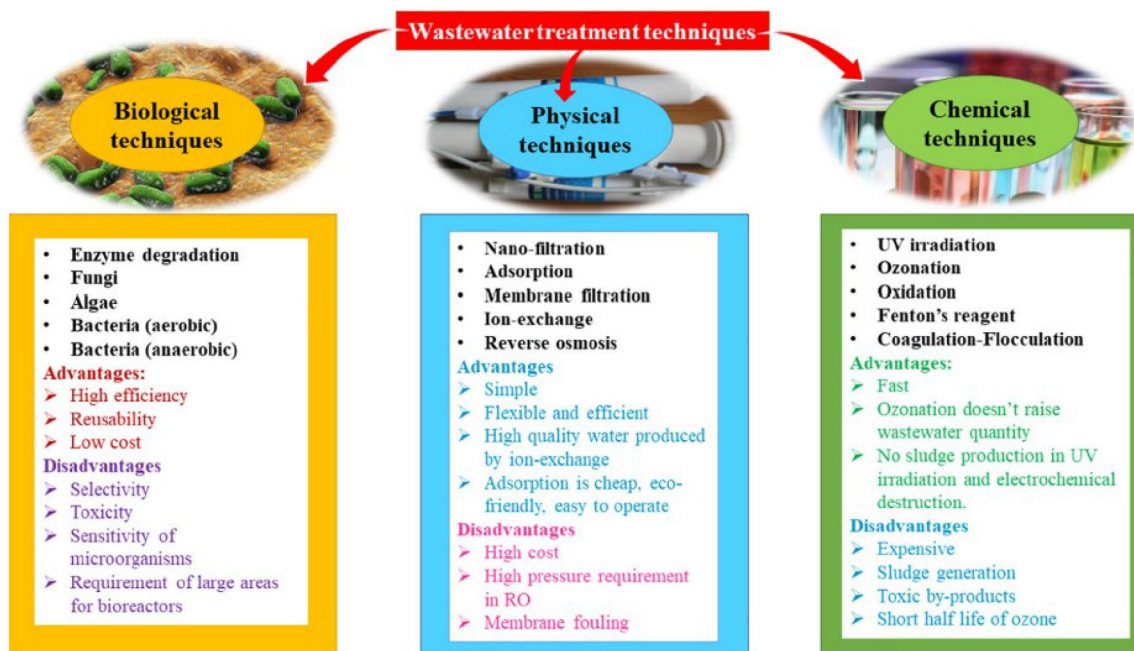
Figure 3. Classification of wastewater treatment techniques.

methods (Agbovi and Wilson 2021; Hameed 2009; Al-Kazragi et al. 2019; Al-Kazragi and Al-Heetimi 2021). A recent study has investigated a variety of microbes (fungi, algae, bacteria, etc.) and enzymes for the biodegradation of colors (Yadav et al. 2021).

Industry is very concerned with the treatment of industrial wastewater in an effort to make their process ecologically friendly. Being the largest consumer of colorants, the effluent from industry contains significant amounts of dyes used in the process, which are toxic, carcinogenic, mutagenic, and pose a serious threat to humans. Researchers have invested a lot of time in removal of dyes from water bodies to reduce the water's environmental risk (Khapre et al. 2022). Different workers have applied several treatment techniques based on their strengths and weaknesses for dye removal from the environment. Due to the disadvantages of other treatment approaches, adsorption is preferred for dye removal from aqueous media (Iwuozor et al. 2021). Adsorption is a versatile method that requires basic infrastructure, economical, simple operation, eco-friendly, and high removal efficiency for a wide range of pollutant concentrations (Ahmadi et al. 2017; Crini et al. 2019; Omidinasab et al. 2018). Adsorption methods can remove diverse contaminants such as organic, inorganic and biological substances that include soluble and non-soluble compounds from water and wastewater (Pandey and Ramontja 2016; Yadav et al. 2021; Okoro et al. 2022; Pandey et al. 2022; Steiger and Wilson 2022). Wang and coworkers have reported the efficiencies of several natural and modified natural adsorbent materials (e.g., fly ash) (Wang et al. 2005), modified coffee waste (Lafi and Hafiane 2016), almond shell (Ardejani et al. 2008), oil palm trunk fiber (Hameed et al. 2008), bentonite (Leodopoulos et al. 2012) for reduction of contaminants in water and wastewater. The development of eco-friendly sorbents that have high uptake and reuse capacity is gaining interest (Pandey et al. 2022). Natural and modified natural adsorbent materials can adsorb organic pollutants such as dyes via H-bonding, ion exchange, complexation, n-π interactions etc., as presented in Figure 4. The adsorption mechanism depends on the nature of the adsorbent and adsorbate properties (surface area and active sites on the surface) and types of interactions that are possible for the adsorbed species (Zhou et al. 2019; Jeong et al. 2022; Gupta et al. 2022).

As mentioned above in Figure 3, several methods can be employed to remove MO dye from aqueous media. Because of its variable efficiency, ease of design, capacity to separate a variety of chemical compounds, economic viability, and selectivity to toxicants, adsorption is preferred over other types of strategies for the mitigation of MO (Chen S et al. 2010; Pandey and Ramontja 2016). Due to the widespread use of MO as an anionic/acidic dye and pH indicator, it was chosen as the key adsorbate for this review paper. This study aims to assess the effectiveness of several types of adsorbents for reducing the levels of MO in water and wastewater. The research of several natural adsorbents and their modified forms can be utilized to remove MO from aquatic systems, with a focus on their adsorbent capacity and comparisons between them. This research is anticipated to shed additional light on MO adsorption processes and the selection of suitable adsorbent types that will serve to benefit practitioners in the field of water treatment technology. The natural adsorbents materials are divided into five classes based on their chemical composition for general comparison and study, as follows:

- Group A: Clays and minerals
- Group B: Bio-sorbents
- Group C: Biochar
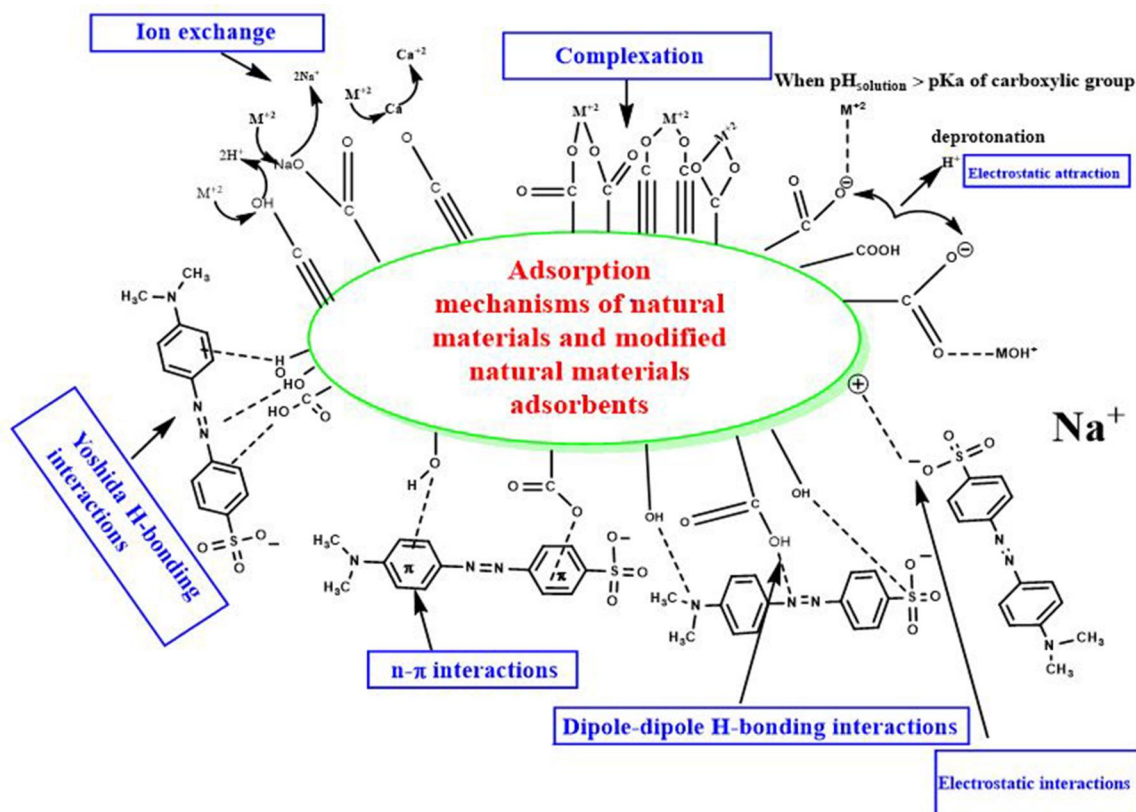- Group D: Activated carbon
- Group E: Composites

Figure 4. Types of potential adsorption mechanisms for various adsorbent-dye systems.

Experimental results of the different adsorbent groups

Group A: Clays and minerals

Clays are a class of microcrystalline minerals that typically contain phyllosilicates with varying levels of structural water. Clays can be substituted for more expensive adsorbents in the water treatment process since they are commonly available and inexpensive as adsorbents. Clays are widely valued as adsorbents because of their high surface area and capacity to adsorb water at interlayer locations. (Iwuozor et al. 2021). Different types of clay minerals are used as adsorbents for the removal of MO from water and wastewater, which includes bentonite (Kan et al. 2011; Al-Heetimi et al. 2012) and kaolin (Al-Ma'amar 2012), among other various types.

The removal of an anionic dye from water onto montmorillonite clay and HCl-activated montmorillonites in fixed bed systems was reported by Teng and Lin (2006). For two weeks at $60\,°C$, $100\,g$ of clay was submerged in a solution of $6\,M$ HCl in a stirred cell at $30\,rpm$. As the clay was activated by acid, the adsorption capacity of montmorillonite clay was significantly increased. Analysis was done on the surface area (BET) and X-ray diffraction profiles. A decrease in the distance between sheets as a result of HCl treatment was also explained by the XRD patterns of the untreated and acid-treated montmorillonite clay. This demonstrated how the raw montmorillonite's surface area ($87.55\,m^2/g$) and average pore size ($6.81\,nm$) were altered to the corresponding values of $114.7\,m^2/g$ and $5.31\,nm$ for the HCl-activated

montmorillonite. The ratio of SiO_2/Al_2O_3, SiO_2/Fe_2O_3, and SiO_2/MgO of the clay increased from 2.9, 33.7, 8.8 to 7.5, 73.1, 8.2 after HCl treatment. It might be as a result of H^+ treatment with acid replacing the Al^{3+}, Mg^{2+}, or Fe^{2+} ions at the cation exchange sites.

The adsorption of MO by calcined layered double hydroxides (LDO) or an anionic clay with Zn/Al molar ratio of 3:1 was studied by Ni et al. (2007). An aqueous solution ($500\,mL$) containing NaOH ($1.6\,mol$) and Na_2CO_3 ($0.15\,mol$) were added dropwise to a solution ($500\,mL$) containing Zn $(NO_3)_2·6H_2O$ ($0.6\,mol$) and Al $(NO_3)_3·9H_2O$ ($0.2\,mol$) (initial Zn/Al $= 3.0$) with vigorous stirring until a final pH of 9.5. The adsorption experiments show the maximum capacity of MO at equilibrium (Q_e) and percentage of adsorption with a fixed adsorbent dose of $0.5\,g\,L^{-1}$ and pH $= 6$ were found to be $181.9\,mg\,g^{-1}$ and 90.95%, respectively, as shown in Figure 5. Adsorption isotherms were correlated by both Freundlich and Langmuir models. Compared to the Langmuir isotherm, the Freundlich isotherm provides a better fit to the experimental data. The fact that $\Delta G°$ values are negative at temperatures between 298 K and 338 K indicates that the adsorption process was spontaneous. The endothermic character of adsorption is demonstrated by the positive value of $\Delta H°$. The enhanced randomness at the solid/solution interface during the adsorption system is indicated by the positive value of $\Delta S°$. The adsorption kinetics of dye ions on an adsorbent surface are better described by the pseudo-second order (PSO) model.

Calcined Lapindo volcanic mud (LVM) as an adsorbent surface was employed to investigate the possibility for
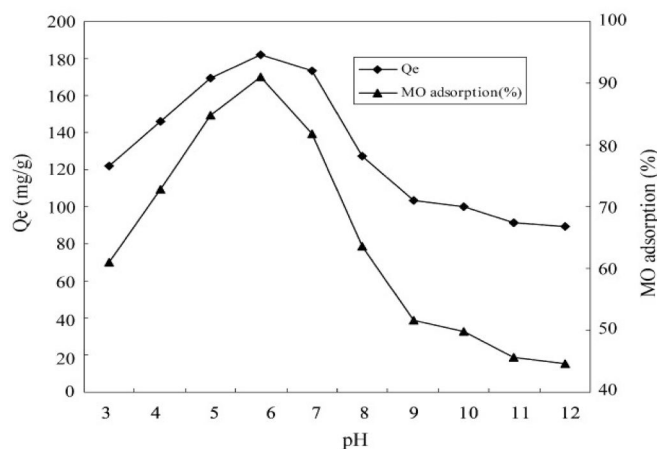
Figure 5. Effect of pH on methyl orange adsorption by Zn-LDO (Ni et al. 2007).
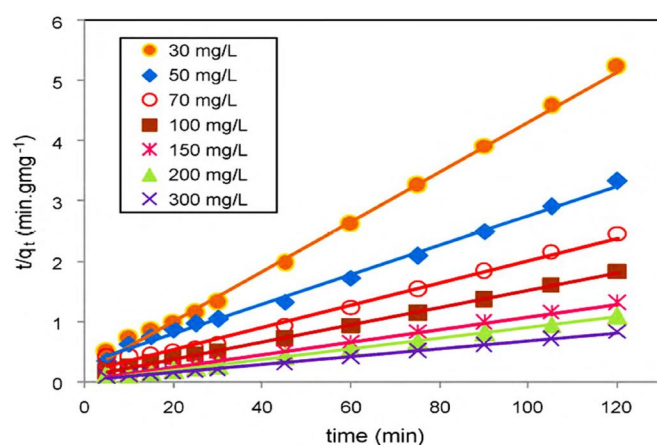

Figure 6. Pseudo-second order (PSO) kinetics for adsorption of MO on LVM (Jalil et al. 2010).

adsorption of MO in its anion form from aqueous solutions, according to Jalil et al. (2010). The physcio-chemical properties of LVM were characterized by using X-ray diffraction (XRD) and field emission scanning electron microscopy (FESEM). Equilibrium conditions were investigated, which includes initial dye concentration, adsorbent mass, contact time, pH, and temperature. The greatest adsorption capacity (66 mg/g) was reached at pH 3, but as the pH of the solution increased, the adsorption capacity decreased. With higher starting dye concentrations (300 ppm), the adsorption capacity increased (150 mg/g) after 30 min of contact. With less adsorbent mass, anionic/acidic dye had a higher adsorption capability. The adsorption capability of MO increases with temperature. Kinetic calculations prove that the adsorption process obeyed the pseudo-second order model (PSO), as shown in Figure 6. The best-fit adsorption isotherm at equilibrium was achieved with the Langmuir isotherm, where the maximum adsorption capacity (q_{max}) was 333.3 mg g^{-1}. The thermodynamic parameters, such as the changes in the standard enthalpy ($\Delta H°$), entropy ($\Delta S°$), and Gibbs free energy ($\Delta G°$) was evaluated, which revealed that the adsorption is endothermic ($\Delta H°$, positive), random ($\Delta S°$, positive) and spontaneous ($\Delta G°$, negative) at high temperature. The results indicate that the LVM could be utilized as

a low-cost alternative adsorbent for the removal of anionic dyes in wastewater treatment.

Bentonite-modified nanoscale zero-valent iron (B-nZVI) was utilized (Chen ZX et al. 2011) to remove the aromatic dye MO from an aqueous solution. The preparation consisted of B-nZVI with an iron/B mass ratio of 1:1, ferric chloride hexa-hydrate (FeCl$_3$.6H$_2$O) (4.84 g) dissolved in 50 mL of miscible liquids (distilled water and absolute ethanol at a volume ratio of 4:1), and addition of treated B (1.00 g), followed by 0.47 M NaBH$_4$ solution (100 mL) added drop-wise into the mixture. The adsorbent surfaces were analyzed by Fourier transform infrared spectroscopy (FTIR), X-ray diffraction (XRD) and scanning electron microscopy (SEM). Various parameters such as MO initial concentration, pH, temperature and dosage were examined. An increase in the rate occurred for the removal of MO when the pH fell. The initial dye concentrations ranged from 100 to 800 mg/L were tested, and the results proved that the removal of MO decreased when the initial concentration of MO increased. The removal efficiency of MO increased as the dosage of B-nZVI increased. The temperature affected the removal of MO when it was raised from 20 to 30^{0}C. Kinetic adsorption studies supported that the removal of MO fitted well to the pseudo first-order (PFO) model. Using B-nZVI, 79.46% of MO was removed, after reacting for 10 min with an initial MO concentration of 100 mg/L (pH = 6.5). The removal rate of MO from actual wastewater was 99.75% upon utilizing B-nZVI.

A new cationic gemini surfactant, glycol bis-N-cetylnicotinate dibromide (GN16-1-16) to modify bentonite was prepared by Kan et al. (2011). Bentonite modified with commercial cetyltrimethylammonium bromide (CTAB) was studied for comparison purposes. The organobentonites were prepared by adding (0.4 g) of powdered bentonite and GN16-1-16 or CTAB (0.05–0.20 mmol) into 50 mL distilled water with stirring at 25– 70 °C for 0.5–3.0 h. The two surfaces were analyzed by FTIR and XRD techniques. The optimum reaction time and temperature were 1 h at 30 °C for GN16-1-16 and 3 h at 70 °C for CTMAB. The GN16-1-16 reacted with bentonite faster than CTAB. As the pH increased, the decolorization rate of the MO solution increased. The decolorization rate and chemical oxygen demand (COD) of MO removal increased with rising GN-Bt and C-Bt dosage and temperature. The decolorization rate and the COD removal of the MO solution were 99.02% and 90.62% for GN-Bt and 80.12% and 75.49% for C-BT. Therefore, GN-Bt was more efficient than C-Bt for removal of MO from aqueous solution.

To remove MO dye from water, (Chen D et al. 2011) modified montmorillonite with cationic surfactant (CTAB), anionic surfactant (sodium stearate; SSTA) and their mixture with montmorillonite (MMT). MMT (4.0 g) was dispensed in 0.25 L of distilled water. Then a certain amount of CTAB was added and the suspension was continuously stirred for 60 min. After that, the anionic surfactant SSTA was added. The above mixture was subjected to mechanical stirring for 4 h in a water bath at 70 °C. The final MMT was separated by centrifugation and washed with 50% (v/v) of water and

ethanol mixture at 60 °C. The resulting sample was dried at 80 °C. The single-cation (CTAB) and single-anion (SSTA) modified with MMT was prepared by mixing Na-MMT with aqueous solutions of either cationic or anionic surfactant. The procedure was the same as anion–cationic surfactants modified MMT. The surface of the adsorbents (CTMAB-MMT, 10SSTA-MMT and CTAB/10SSTA-MMT) were characterized by FT-IR spectroscopy, XRD and thermogravimetry-differential thermal analysis (TG-DTA). The effect of different factors on the adsorption of methyl orange dye by CTAB/10SSTA–MMT included contact time, temperature and pH. The maximum adsorption capacity of MO onto surfactant modified MMT samples was observed at 60 min which is fixed as the equilibrium contact time. Based on the correlation coefficients (R^2) for the PSO kinetic model are between 0.9938 and 0.9998, the adsorption system of MO onto CTMAB/10SSTA–MMT fits the PSO kinetic model. As the pH of the dye solution increases from pH 3 to 10, the adsorption capacity of the dye onto CTAB/10SSTA–MMT decreases. The equilibrium adsorption capacity of CTAB/10SSTA–MMT was found to decrease from 57.14 mg g^{-1} to 51.28 mg g^{-1} upon raising the temperature from 30 °C to 60 °C. The analysis of equilibrium parameters for the adsorption of MO onto MMT and surfactant modified MMT was investigated by the Langmuir and Freundlich isotherm models. The results showed that the Langmuir model provides a better fit than that of the Freundlich model the adsorbent materials investigated. The maximum adsorption capacity of MO onto MMT, CTAB-MMT, 10SSTA-MMT and CTAB/10SSTA-MMT was found to be 24.00, 128.21, 42.37 and 149.25 mg/g, respectively. The standard difference for the various thermodynamic functions ($\Delta G°$, $\Delta H°$, and $\Delta S°$) were estimated with negative values at the experimental temperatures studied. This trend suggests that MO adsorption onto CTAB/10SSTA–MMT is spontaneous, exothermic and reveals a decrease in the degree of freedom of the adsorbed molecules. The adsorption experiments revealed that CTAB/10SSTA-MMT had the largest adsorption capacity compared with CTAB-MMT and 10SSTA-MMT.

The adsorption of MO from wastewater onto a low-cost adsorbent (acid-activated bentonite) was investigated by Leodopoulos et al. (2012). The acid activation of the bentonite was performed with 3 M H_2SO_4 under reflux conditions. The unmodified and modified surfaces were characterized by FTIR spectroscopy. The specific surface area (BET) of the bentonite clay was calculated by adsorption–desorption of nitrogen at 77.4 K. The specific surface area of raw bentonite was 103 m^2 g^{-1} and increased to 355 m^2 g^{-1} after treatment with H_2SO_4. The effect of pH, initial azo dye concentration and ionic strength on the adsorption efficiency was also investigated. The adsorption of MO decreased with an increasing pH from 77% (q_e, MO = 8.37 mg/g) to 30% (q_e, MO = 3.27 mg/g). An increase in the ionic strength increased the removal of MO from 49.4% to 59.9%. An increase of the initial concentration of anionic/acidic dye from 10 to 50 mg/L increased the amount adsorbed from 3.6 to 14.8 mg g^{-1}. The Langmuir and Freundlich isotherm equations were employed to evaluate the equilibrium

adsorption data of MO, where the experimental results revealed that the best-fit results were achieved with the Freundlich model, based on the correlation coefficient (R^2 = 0.9). The PSO model was fitted to the kinetic adsorption profiles.

The adsorption behavior of MO from aqueous solution onto Iraqi bentonite was studied by (Al-Heetimi et al. 2012). The influence of various parameters such as initial concentration, adsorbent amount, ionic strength and temperature were tested. The amount of dye adsorbed increases as dye concentration rises (10–40 ppm) and decreases as the bentonite dose rises (0.05–0.35 g/L). With an increase of the ionic strength and temperature, the amount of dye adsorbed decreased. The Langmuir isotherm provided a good fit for the equilibrium studies, which were conducted using the Temkin and Langmuir isotherm models. Thermodynamic parameters were also assessed, where a low negative value of $\Delta G°$ indicates that the adsorption process is both feasible and spontaneous. The exothermic nature of the adsorption process is indicated by the negative value of $\Delta H°$ (−29.98 kJ/mol). The decreasing randomness at the solid/liquid interface during the adsorption process is suggested by the negative value of $\Delta S°$ (−83.31 J/mol. K).

Zeolites of the X-type and A-type were created from fly ash (Das et al. 2012) using alkali fusion, followed by hydrothermal treatment that were used to remove MO from aqueous media. In order to prepare a zeolite, sodium hydroxide and fly ash were calcined and treated with HCl, followed by combination and fuzing in a stainless-steel tray over a range of temperatures for one hour. The weight-to-weight ratio of sodium hydroxide to fly ash ranged from 1.0 to 1.5. The synthesized zeolite was characterized using different techniques such as XRD and SEM. Langmuir and Freundlich isotherms were used for fitting the experimental data in adsorption studies, the adsorption equilibrium results were found to have a best-fit with the Freundlich isotherm model. It was observed that removal of the acidic dye increased from 53% to 72% as the solution pH increased from pH 2 to 10. The exothermic nature of the adsorption process at lower temperatures is indicated by the more negative values of the standard Gibbs free energy difference ($\Delta G°$; −3.8, −5.3, and −7.5 kJ/mol) and enthalpy change $\Delta H°$ (−20.85 kJ/mol). The diminishing randomness on the surfaces of the adsorbents is demonstrated by the negative values of standard entropy change $\Delta S°$ (−90.61 J/mol K).

The adsorption of MO onto kaolinite clay was investigated by Al-Ma'amar (2012). The adsorption isotherm profiles were followed by the Freundlich isotherm, where multi-layers were formed and the uptake process was a combination of adsorption and absorption (sorption). In some cases, desorption occurred and the determination of thermodynamic factors reveal that the adsorption process was exothermic ($\Delta H°$, negative value), ordered ($\Delta S°$, negative value), and non-spontaneous ($\Delta G°$, positive value) over a narrow temperature range (298–328K). The adsorption kinetics was evaluated by several models: PFO, Weber-Morris and Elovich models. The desorption process occurred at higher MO concentrations and the activation energy (E_a,

4.956 kJ/mol) is low, which indicates that the sorption is relatively rapid.

To enhance the capacity of MO to be adsorbed from aqueous solutions, (Tang *et al.* 2012) treated vermiculite mineral clay with cationic surfactant (CTAB). 50 g of vermiculite clay was put into a beaker, 500 mL of distilled water was added until the clay becomes fully wet and dispersed, and the equivalent of 100% cation exchange capacity (CEC) of CTAB surfactant was then added. The structural characteristics of vermiculite and CTAB-vermiculite were tested through SEM, which revealed that the interlayer of the CTAB-vermiculite becomes larger and unlike the original clay material. The effects of the material dosage, contact time, the anionic dye concentration, and pH on the adsorption process of MO were studied. In Figure 7, there was a greater percentage of adsorption with longer shaking times. An equilibrium condition was achieved for the MO adsorption onto the CTAB-vermiculite takes around 30 min. As the dosage of the adsorbent was increased, the extent (%) of adsorption also increased. It was determined that MO was effectively adsorbed onto the surface of CTAB-vermiculite even at low pH conditions.

The effectiveness of kaolinite (KAO) and metakaolinite (MK) as an effective adsorbent for the removal of MO in aqueous media was previously reported (Fumba *et al.*, 2014). The KAO and MK surfaces were characterized using various spectral techniques such as XRD and FT-IR, whereas the surface area was calculated using the BET method. The various factors that influence the adsorption process, including the contact time, adsorbent dosage, pH, and initial dye concentration were studied. An account of the experimental findings indicates that the amount of azo dye species that were adsorbed increased with greater contact time and reached equilibrium by 15 min for KAO and 10 min for MK. At a pH of 2.5, the maximum level of adsorption was estimated. As the adsorbent dosage increased, a decrease in the MO removal occurred, whereas the level of adsorption increased with greater initial azo dye concentration. Three isotherm models (Langmuir, Freundlich and Dubinin-Kaganer-Radushkevich D-K-R) were used to describe the experimental data. The experimental results reveal that the Langmuir isotherm provided a better fit over the Freundlich and D-K-R isotherm models, according to their R^2 values
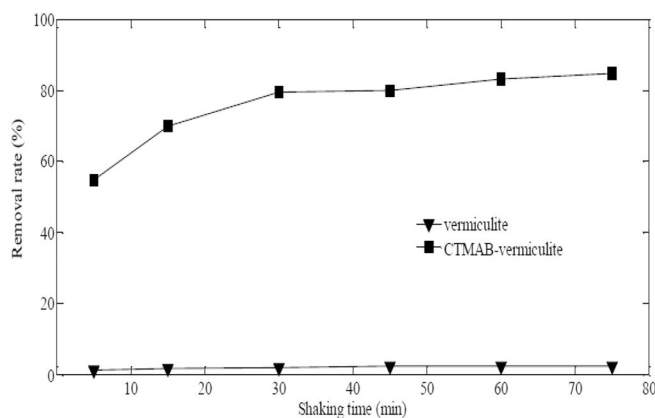
(cf. Figure 8). The PFO, PSO, Elovich, intraparticle diffusion and mass transfer kinetic models were tested to gain insight on the mechanism of dye adsorption onto KAO and MK. The kinetic data revealed that chemisorption was the rate-limiting step and that the PSO kinetic model was well suited as revealed by Figure 9. According to this study, the dye adsorption efficiency according to Q_e was greater for MK over KAO.

The NiFe layered double hydroxides (LDHs) with various mole ratio of Ni/Fe (4:1, 3:1, 7:3 and 1:1) were prepared by Lu *et al.* (2016) *via* employing a co-precipitation method to remove the anionic form of MO. 20 mL of $Ni(NO_3)_2.6H_2O$ and $Fe(NO_3)_3.9H_2O$ solution were added into a vigorously stirred ammonia solution (100.0 mL, 0.5 M) in a drop-wise manner. The suspension (yellow brown precipitate) was stirred mechanically for a further 18 h at 65 °C, then centrifuged and washed thoroughly with deionized water, and dried overnight at 60 °C under vacuum. The adsorbent surface was characterized using XRD, FT-IR, SEM and transmission electron microscopy (TEM). Ni_4Fe_1-LDH can remove more than 92% of MO in 10 min at the 10 mg/L MO initial concentration. The adsorption property of Ni_4Fe_1-LDH was tested by the Langmuir and Freundlich isotherm adsorption models. The corresponding equilibrium results reveal that the adsorption behavior of this new adsorbent is accounted for by the Langmuir isotherm, which suggests that the LDH surface is homogeneous with a monolayer adsorption mechanism. Moreover, the theoretical Langmuir maximum adsorption capacity of Ni_4Fe_1-LDH was found to be 205.76 mg/g. The PSO model accounted for the adsorption kinetics profile of the anionic/acidic dye onto Ni_4Fe_1-LDH, in contrast to the poor agreement obtained by the PFO model. The results indicate that the adsorption process is chemisorption in nature and the Ni_4Fe_1-LDH represent a promising adsorbent for the removal of MO dye from wastewater.

Kaolinite clay was treated with 2 M oxalic acid (Sejie and Nadiye-Tablebiruka 2016) in order to examine its ability to remove the MO azo dye from water. The clay was leached with 2 M oxalic acid for 2 h at 371 K and further examined using spectroscopy (FTIR, SEM, and X-Ray Powder Diffraction (XRPD)) techniques. The kinetic adsorption
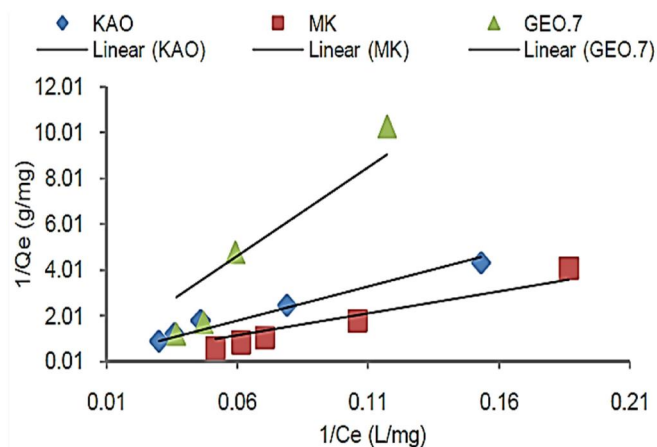

Figure 7. Effect of shaking time on removal rate of MO (Tang *et al.* 2012).

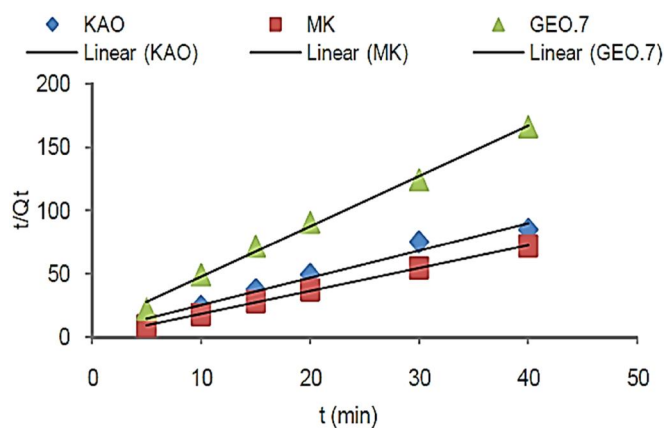**Figure 8.** Linear plots of the Langmuir model (Fumba *et al.* 2014).

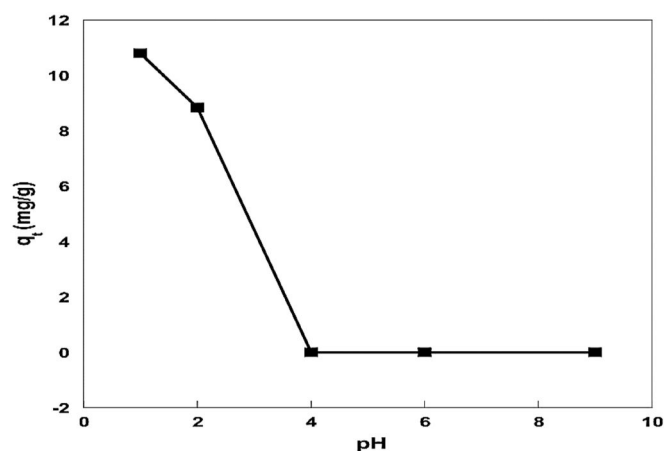**Figure 9.** Pseudo-second order (PSO) plots for MO adsorption onto KAO, MK and GEO.7 (Fumba *et al.* 2014).

Figure 10. Effect of pH on the equilibrium adsorption of MO onto bentonite (Bellifa *et al.* 2017).

Figure 11. Fitting of kinetic data to the PSO kinetic model onto bentonite (Bellifa *et al.* 2017).

studies agreed well with the PSO model. The adsorption of MO onto the modified clay rises with greater dye concentration, falling pH, and reduced temperature. Two isotherm models (Freundlich and Temkin) were used to evaluate the equilibrium data and the results reveal that the Freundlich model has the best-fit result, which indicates the heterogeneity of the clay surface.

In study by Bellifa *et al.* (2017) an Algerian clay of the bentonite type was used to study the adsorption of MO as a model anionic dye from aqueous media. Acid was used to activate the bentonite and a study of the variables that impact the adsorption efficiency are listed, as follows: contact time, adsorption kinetics, adsorbate concentration, and pH. In less than 60 min, the MO adsorption equilibrium on the bentonite was reached. In the pH range of 1.0–4.0, the adsorption of azo dye fell significantly (cf. Figure 10) and then stayed constant between pH 4.0–8.0. The adsorption of MO rises as its concentration increases in the aqueous solution. The experimental results were best-fit by the Freundlich and Langmuir isotherm models, which suggest the formation of a monolayer followed by multilayer adsorption. The adsorption kinetics agreed with the PSO equation as revealed in Figure 11 for the adsorption of MO dye, in agreement with a chemisorption mechanism that occurs *via* electrostatic attraction. Negative values of $\Delta G°$ suggested
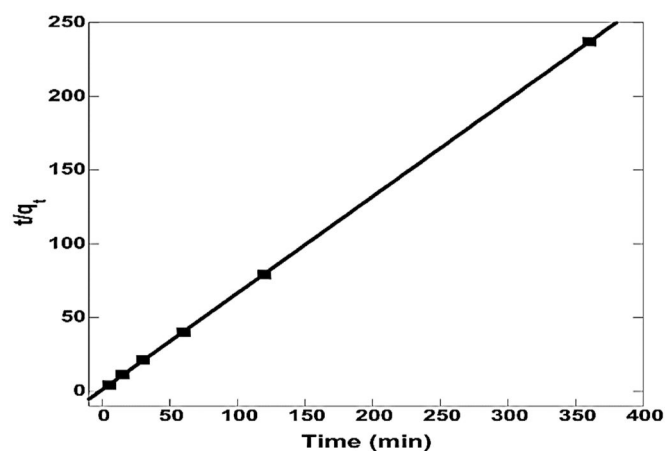
spontaneity of the adsorption process, whereas a positive value of $\Delta H°$ (5.28 kJ/mol) showed that the adsorption system was endothermic. The calculated $\Delta S°$ is positive (+0.0189 kJ/mol) corresponds to a greater degree of freedom at the solid/solution interface of the overall adsorption process. The findings of the experiment reveal that the adsorbents may be reused for the removal of azo dye from aqueous media.

In 2018, (Zayed *et al.* 2018) investigated the effectiveness of the adsorption properties of some Egyptian clay materials. Organic Matters-Rich Clays (OMRCs) were calcined at 500 °C for 4 h. The effectiveness of MO removal from both OMRCs and its calcined derivative (COMRC) was then assessed under various experimental conditions. The two adsorbent surfaces were characterized by XRD, FT-IR, SEM and Energy Dispersive X-Ray (EDX) spectroscopy. The optimum removal capacity was noted at pH 2.0 and 3.0 for OMRC and COMRC surfaces with efficiency 96.4%, 96% and 92.9%, 81.1%, respectively. The removal capacity of MO by the OMRC and COMRC was greater as the adsorbent dosage increased from 0.05 to 0.2 g. The adsorption kinetics of two adsorbents were well represented by the PSO model ($R^2 > 0.999$), where neither the adsorbent's intra-particle diffusion process acted as a rate-limiting step in the acidic adsorption process. The adsorption properties showed that the Freundlich and Langmuir models can account for the adsorption equilibrium isotherm profiles of the OMRC and COMRC materials. Although the COMRC revealed a lower MO maximum adsorption capacity ($q_{max} = 34.48$ mg/g) than the OMRC ($q_{max} = 41.67$ mg/g) system, this trend was attributed to the lower BET surface area of COMRC versus OMRC. In turn, these clays can be employed as low-cost materials for removal of an acidic dye from aqueous media.

In the study by Tetteh *et al.* (2019) the ability of muscovite clay was evaluated to remove MO from aqueous media. Studies of MO adsorption were completed at 303, 323 and 343 K and variable pH. After 30 min, equilibrium adsorption conditions were achieved and the Langmuir isotherm model provided an estimate of the monolayer adsorption capacity (13.00 mg/g) for dye ions at 303 K. With $R^2 > 0.99$ and negative activation energy values supporting the

physisorption process, the PSO kinetic model accurately predicted the rate of adsorption, while an analysis of the thermodynamic parameters suggested that the adsorption system was endothermic ($\Delta H^{\circ} = +8.77$ kJ/mol) but, the positive entropy change ($\Delta S^{\circ} = + 2.73$ J/mol. K) resulted in negative values for ΔG°. Over a pH range from 3.3 to 7.0, the MO dye adsorption increased, while a decrease was noted from pH = 8.0 to 10.0. This trend relates to electrostatic repulsion between anionic sites on the dye and the negatively charged sites on the adsorbent surface.

The effectiveness of acid treatment on Brazilian natural bentonite for the adsorption of anionic dye (MO) was examined by Fernandes et al. (2020). Acid functionalization in natural bentonite (RF) was carried out with HCl (13.04 M) and H_2SO_4 (18.38 M) acids (denoted as RF1 and RF2, respectively) under constant temperature (90° C) for 2 h. The untreated and treated bentonite were characterized by chemical analysis, mineralogy, particle size, and thermal behavior with the associated mass losses. The adsorption capacity with the MO dye was tested by the effects of the initial concentration of MO and the contact time. The acid treatment was efficient for increasing the adsorption capacity of the anionic dye, and the Q_{max} values obtained were 2.2 mg/g, 67.4 mg/g and 47.8 mg/g for RF, RF1 and RF2, respectively. The Langmuir, Freundlich, Dubinin-Astakhov (D-A), Dubinin-Radushkevich (D-R) and Sips models were used to infer surface properties of the natural and acidified bentonite with the anionic dye. The best fit results to the adsorption isotherms were obtained by the Sips model, according to the experimental results. Thus, the adsorption of the anionic form of the MO dye increased by up to 8000% by employing the acid-functionalized bentonite. The electrostatic interaction between the anionic dye ions and the bentonite surface served as a demonstration of the improved adsorption capacity of acidified adsorbent.

The adsorption of MO from aqueous solution onto natural and CTAB modified Kaolinite clays as a potential cheap adsorbent was studied by Kourim et al. (2021). The organoclay was prepared by adding 10 g of purified clay to 250 mL of CTAB solution (0.02 M) while the mixture was stirring at room temperature for 24 h. The kinetics and thermodynamics of the adsorption experiments were investigated, as well as equilibrium adsorption isotherms. For the characterization of the adsorbent were determined such as pH, the specific surface area, the pH at the point-of-zero-charge (pH_{pzc}) and the cation exchange capacity. Different factors were tested such as contact time, initial dye concentration, dosage of adsorbent surfaces, pH of the solution and temperature. As the dosage of the adsorbent is increased, less MO was adsorbed. The amount of anionic/acidic color that adheres to the clay increases as the pH was reduced from 11 to 2. With an increase in the starting concentrations and contact duration, the equilibrium adsorption capacity (q_e) of the adsorbents rose. The data of adsorption process followed the PSO model and the equilibrium isotherm was best-fit to the Langmuir isotherm model. The calculated standard free energy changes (ΔG°) were negative and highlight the spontaneous nature of the adsorption process. The negative value

of ΔH° indicated an exothermic adsorption process. The positive value for ΔS° indicates that the degree of freedom increased during dye adsorption at the adsorbent-liquid interface. Table 2 lists the adsorption capacities of the numerous minerals and clays, both natural and artificial that have been employed to remove MO from solutions. By comparison, Table 3 lists the kinetic parameters according to various kinetic models (PFO, PSO) and thermodynamic parameters for adsorption of MO dye onto minerals and clays.

Group B: Bio-sorbents

Bio-sorbents are materials of biological origin that were treated thermochemically and used for the removal of toxic compounds from the environment through adsorption. Bio-sorbents are very popular adsorbents as most of them are low-cost and abundant materials. Recently, agricultural and food wastes are widely used as bio-sorbents. Researchers have tested various bio-sorbents such as tea waste, peanut and almond shells, sugarcane bagasse, rice husk, corn cob, orange peel etc. for water and wastewater treatment and have found positive results (Bhattacharjee et al. 2020).

The adsorption properties of MO on the starches of kudzu, sweet potato, corn, rice, wheat, potato, and snake gourd were studied by Boki et al. (1991). Because phosphate esters are present, no MO adsorption was seen on potato or snake gourd starch. The differences in amount of MO adsorbed on kudzu and sweet potato starches could be explained by the number of neutral hydrophilic sites rather than surface area, pore volume, pore size distribution, glucose-6-phosphate and amylose content. Adsorption isotherms were described by both the Langmuir and Freundlich models in all others, which assumes that methyl orange was confined to a monolayer onto the heterogeneous surface of the starches.

The equilibrium and kinetics of MO adsorption from aqueous solutions onto banana and orange peels were investigated by Annadurai et al. (2002). For the adsorption of MO using banana peels, the Freundlich model provided a slightly better match than the Langmuir model, but exactly reversed using orange peels. The amount of MO adsorption was maximized at pH 6–7 up to 17.2 mg/g using banana peel and at pH > 7 up to 15.8 mg/g using orange peel, which indicated an alkaline pH was favorable for the azo dye (MO) adsorption. After 20 min of contact, it was found that the intraparticle diffusion of dye molecules within the particles was rate-controlling in this adsorption process. The parameters for the kinetics of adsorption, according to the Lagergren rate constant and the intraparticle rate constant were estimated.

In 2007, Mittal et al. (2007) used de-oiled soya and bottom ash a waste of thermal power plants as a promising low-cost adsorbent for removal of toxic dye MO from wastewater. The effects of amount of dye and adsorbent, pH solution, sieve diameters, temperature, and column studies were investigated. Adsorption of acidic dye was tested for both adsorbents over a pH range of 2–10, and the

Table 2. Adsorption performance of MO by Group A adsorbents.

Adsorbent name	q_{max} (mg/g)	pH	Temp. (°C)	Model for q_{max} determination	Reference
HCl-activated montmorillonites	–	–	–	–	(Teng and Lin 2006)
Calcined layered double hydroxides (LDO) with Zn/Al	285.70 75.16	6.0	56	Langmuir Freundlich	(Ni et al. 2007)
Calcined Lapindo volcanic mud	333.33	3.0	30	Langmuir	(Jalil et al. 2010)
Bentonite-supported nanoscale zero-valent iron	–	–	–	–	(Chen ZX et al. 2011)
Glycol bis-N-cetylnicotinate dibromide (GN16-1-16) modified bentonite	–	–	–	–	(Kan et al. 2011)
Montmorillonite	24,00	–	30	Langmuir	(Chen D et al. 2011)
CTAB modified montmorillonite	128.21	–	30	Langmuir	(Chen D et al. 2011)
Sodium stearate modified montmorillonite	42.73	–	30	Langmuir	(Chen D et al. 2011)
CTAB and sodium Stearate modified montmorillonite	149.25	3	30	Langmuir	(Chen D et al. 2011)
Humic acid activated bentonite	33.80	–	25	Langmuir	(Leodopoulos et al. 2012)
Iraqi bentonite	0.93	–	25	Langmuir	(Al-Heetimi et al. 2012)
Zeolites	0.013	–	–	Freundlich	(Das et al. 2012)
Kaolinite clay		–	–	Freundlich	(Al-Ma'amar 2012)
CTAB modified vermiculite clay	–	3	–	–	(Tang et al. 2012)
Kaolinite	1.25	2.5	–	Langmuir	(Fumba et al. 2014)
Metakaolinite	3.08	2.5	–	Langmuir	(Fumba et al. 2014)
NiFe layered double hydroxides	205.76	–	–	Langmuir	(Li et al. 2016)
Kaolinite clay treated with Oxalic acid	5.77	12	25	Freundlich	(Sejie and Nadiye-Tablebiruka, 2016)
Bentonite	118.00 0.85	–	–	Langmuir Freundlich	(Bellifa et al. 2017)
Calcinated Egyptian clay	34.48	3	–	Langmuir	(Zayed et al. 2018)
Muscovite clay	13.00	–	30	Langmuir	(Tetteh et al. 2019)
Acid modified bentonite	74.23	–	–	Sips	(Fernandes et al. 2020)
CTAB modified kaolinite	855.07	–	50	Freundlich	(Kourim et al. 2021)

Table 3. Kinetic parameters of pseudo-first order (PFO), pseudo-second order (PSO) models and thermodynamic parameters for the adsorption of MO dye by Group A adsorbents.

Adsorbent name	k_1 (min^{-1})	k_2 (g/mg min)	Temp. (°C)	$\Delta H°$ (kJ mol^{-1})	$\Delta G°$ (kJ mol^{-1})	$\Delta S°$ (J mol^{-1} K^{-1})	Reference
HCl-activated montmorillonites	–	–	–	–	–	–	(Teng and Lin 2006)
Calcined layered double hydroxides (LDO) with Zn/Al	–	4.49	25	3.41	−10.35	46.21	(Ni et al. 2007)
Calcined Lapindo volcanic mud	0.15	0.0014	30	159.88	2.43	0.52	(Jalil et al. 2010)
Bentonite-supported nanoscale zero-valent iron	–	–	–	–	–	–	(Chen ZX et al. 2011)
Glycol bis-N-cetylnicotinate dibromide (GN16-1-16) modified bentonite	–	–	–	–	–	–	(Kan et al. 2011)
Montmorillonite	6.89×10^{-2}	3.84×10^{-3}	30	–	–	–	(Chen D et al. 2011)
CTAB modified montmorillonite	3.61×10^{-2}	1.49×10^{-3}	30	–	–	–	(Chen D et al. 2011)
Sodium stearate modified montmorillonite	6.46×10^{-2}	2.63×10^{-3}	30	–	––	–	(Chen D et al. 2011)
CTAB and sodium Stearate modified montmorillonite	4.78×10^{-2}	2.33×10^{-3}	30	−35.04	−7.55	−91.25	(Chen D et al. 2011)
Humic acid activated bentonite	0.02	0.03	25	––	–	––	–
Iraqi bentonite	–	–	25	−29.98	−5.20	−83.31	(Al-Heetimi et al. 2012)
Zeolites	–	–	–	−20.85	−90.61	–	(Das et al. 2012)
Kaolinite clay	–	–	25	−9.48	+2818.50	−9.49	(Al-Ma'amar 2012)
CTAB modified vermiculite clay	–	–	–	–	–	–	(Tang et al. 2012)
Kaolinite	1.00	1.14	–	–	–	–	(Fumba et al. 2014)
Metakaolinite	0.00	0.92	–	–	–	–	(Fumba et al. 2014)
NiFe layered double hydroxides	–	–	–	–	–	–	(Li et al. 2016)
Kaolinite clay treated with Oxalic acid	–	–	–	–	–	–	(Sejie and Nadiye-Tablebiruka 2016)
Bentonite	–	–	15	5.28	0.158	18.90	(Bellifa et al. 2017)
Calcinated Egyptian clay	–	0.03	–	–	–	–	(Zayed et al. 2018)
Muscovite clay	0.01	13.51	30	13.00	−0.98	2.73	(Tetteh et al. 2019)
Acid modified bentonite	0.01	8.3×10^{-3}	–	–	–	–	(Fernandes et al. 2020)
CTAB modified Kaolinite	0.06	0.03	30	−9293.70	31110.69	−20.40	(Kourim et al. 2021)

adsorption was shown to be highest at pH 3. Adsorption was found to decrease with increasing pH. The highest dye adsorption was attained at 0.1 g of bottom ash and 0.05 g of de-oiled soya, and these were used for all experiments. In all cases, the adsorption of dye increases with an increase in the amount of adsorbents. The amount of dye that is absorbed increases as the mesh size increases, in line with surface area effects. As such, the bottom ash (100 BSS) and de-oiled soya (36 BSS) mesh sizes were selected for further research. Adsorption of the MO dye over two adsorbent surfaces were applied through the Langmuir and Freundlich isotherm models and possibility of the process is achieved in both the cases. The fitted isotherm lines of de-oiled soya and bottom ash are shown in Figures 12 and 13. Thermodynamic parameters such as standard enthalpy, standard entropy and standard Gibb's free energy were also
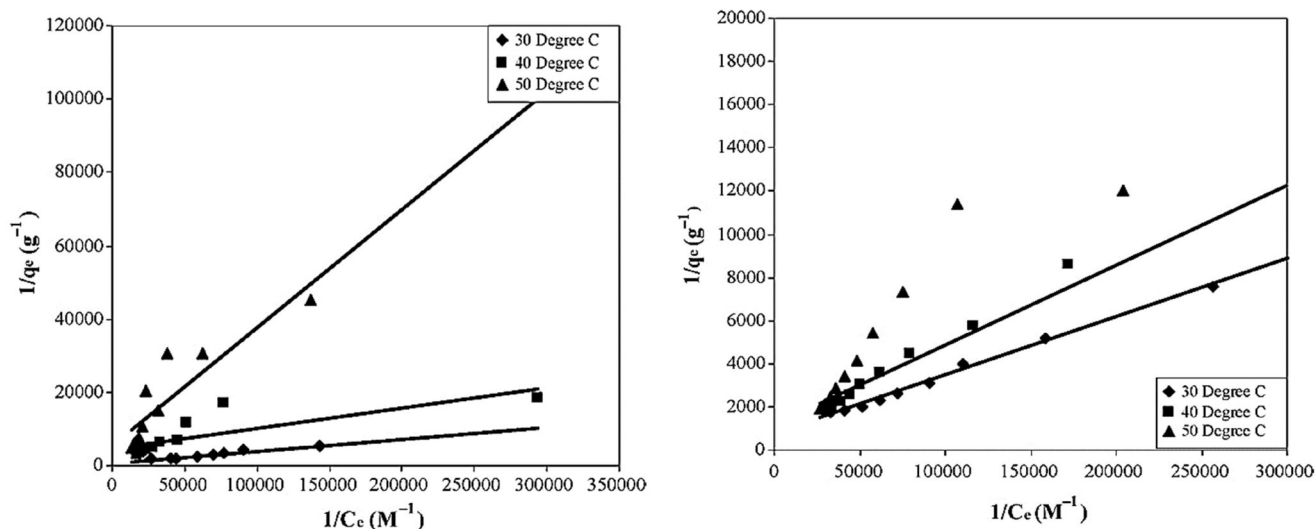
Figure 12. Langmuir adsorption isotherms for methyl orange–de-oiled soya and bottom ash systems (Mittal *et al.* 2007).
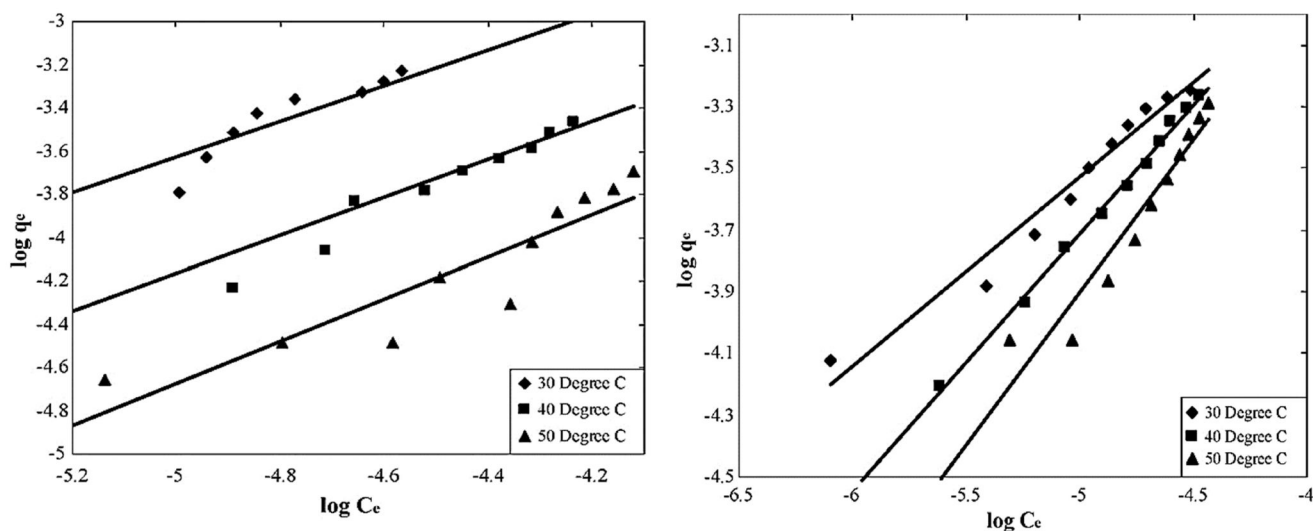

Figure 13. Freundlich adsorption isotherms for methyl orange–de-oiled soya and bottom ash systems (Mittal *et al.* 2007).

studied through these adsorption models. The calculated values for thermodynamic parameters clearly appear that the adsorption process is exothermic in nature (ΔH°, negative), random (ΔS°, positive) and spontaneous (ΔG°, negative) for the two adsorbents. The kinetics results suggest that the removal of dye occurs *via* particle diffusion for bottom ash and *via* film diffusion for the case of de-oiled soya. In the column operations, maximum adsorption capacities of both adsorbents are found as 3.618 mg/g for the bottom ash and 16.664 mg/g for the de-oiled soya, while percentage saturations are found to be 98.61% for bottom ash and 99.8% for de-oiled soya.

Boiler fly ash from a palm oil mill was employed (Okoronkwo *et al.* 2008) for the adsorptive removal of the anionic form of MO dye. The MO concentration (250.0 mg/L) rose with passing time and peaked near 20 min. The Freundlich and Langmuir isotherms were used to simulate the adsorption equilibrium, and the results show that the adsorption isotherm shows good agreement with the Freundlich model. The experiment was also tested using the

PFO and PSO models and the kinetic data of MO was described very well by the PSO model with correlation coefficient (R^2) value of 1.0 and rate constant (k_2) value of 1.6 g mg^{-1} min^{-1}.

In 2010, Atmani *et al.* (2010) reported the efficacy of utilizing skin from almonds (SA), a novel agricultural adsorbent surface, for the eradication of the acidic dye MO. 1.0 g of SA was treated by three different types of chemical treatments: acidic (H_2SO_4), alkaline (NaOH) and salt treatment ($MgCl_2$), which were considered at two levels, 50 and 70 °C for the temperature, 2 and 4 h for the contact time, and 1 and 2 M for the reagent concentrations. The SA treatment with salt solution and alkaline solution reduced the ability of the acidic dye to adsorb, while the salt solution treatment increased the ability of the acidic dye to adsorb from 37.5% to 78.1% (2 M, $T = 70$ °C and 4 h treatment time). Different parameters were studied such as contact time, temperature, dye concentration and particle size. With longer contact times, the adsorption capacity rose until it reached its peak of 13.5 mg/g in 100 min at 23 °C. The quantity of MO

adsorbed rose from 3.2 to 15 mg/g and from 4.6 to 31.3 mg/g as the initial dye concentration increased from 5 to 40 mg/L for natural skin almonds (NSA) and treated skin almonds (TSA), respectively. According to the effects of increasing surface area, a reduction in adsorbent particle size from 850 to 500 μm resulted in an increase in the adsorption capacity from 10.9 to 13.5 mg/g. Adsorption equilibrium was found to follow a Freundlich isotherm for both the untreated and treated SA systems. To examine the kinetic profiles, two kinetic models (PSO and the Elovich equation) were applied. According to the kinetic investigations, the PSO model accounted for the adsorption behavior. The activation energy (E_a) values were estimated as (-28.19 and -20.95 kJ/mol) for MO-NSA and MO-TSA, respectively, suggesting that dye adsorption process onto NSA and TSA was exothermic. Furthermore, these low E_a values demonstrated that physisorption governed the adsorption process.

In 2013, a study by Deniz (2013) reported on the removal of MO from aqueous media using the almond shell, Prunus amygdalus L. On the removal of dye, tests were done on the effects of contact time, ionic strength, adsorbent concentration, mesh size, dye concentration, pH, and temperature. As the pH rose from 3 to 9, it was observed that the MO removal fell from 20.63 to 14.57 mg/g. The dye removal enhanced with decreasing the adsorbent particle size and ionic strength. The adsorption capacity of adsorbent surface increased from 23.42 to 40.21 mg/g with an increase in the initial azo dye concentration from 50 to 100 mg L^{-1}. According to the correlation coefficient ($R^2 = 0.99$), the adsorption kinetics obeyed the PSO kinetic model. The equilibrium data presented the best match to the Langmuir isotherm with maximum adsorption capacity of 41.34 mg g^{-1} at 293 K. Thermodynamic parameters such as the standard Gibbs free energy change ($\Delta G°$), standard enthalpy change ($\Delta H°$) and standard entropy change ($\Delta S°$) were studied, where a negative ($\Delta G°$) at all temperatures highlight the feasibility and spontaneous nature of the adsorption system. Likewise, a decrease in the values of ($\Delta G°$) with increasing temperature proves that the adsorption process was more favorable at lower temperatures. The negative value of ($\Delta S°$) implies a decreased randomness at the adsorbent surface, while the negative magnitude of ($\Delta H°$) indicates that the adsorption process was exothermic.

In 2013, Haddadian et al. (2013) used dragon fruit foliage (DFF) as an adsorbent for the removal of methyl orange from aqueous solution. The bio-sorbent was characterized using FT-IR spectroscopy and scanning electron microscopy. The influence of the initial dye concentration, contact time, pH, temperature, dosage of bio-sorbent and ionic strength were evaluated. As the pH rose to pH 6, the biosorption (%) of DFF increased, indicating that the optimum pH for dye biosorption is 6.0. The biosorption capacity increased from 2.984 to 21.051 mg g^{-1} with increasing the initial concentration of anionic dye from 12.5 to 250 ppm. The MO removal (%) raised with an increase in bio-sorbent dosage. The highest dye removal (80%) occurred when using 1.4 g of DFF at pH 6 within 60 min. The biosorption capacity of the anionic or acidic dye increased with increasing temperature between 298 K to 328 K. While increasing the ionic strength, the dye biosorption decreased sharply. The Freundlich model was found to best describe the adsorption isotherm when it was compared to the Langmuir model. The PSO kinetic model provided a good fit for the kinetic investigation. Thermodynamic parameters were also determined and the experimental results showed negative values of ($\Delta G°$) at all temperatures studied, which proved that the biosorption process was practical and feasible. The positive values of ($\Delta H°$) indicate that the biosorption system is endothermic. The positive values of entropy change ($\Delta S°$) suggest increased randomness at the solid/liquid interface during the biosorption process of the dye system.

In 2014, Su et al. (2014) used CTAB to modify wheat straw (WS). To prepare organo-wheat straw, five grams natural wheat straw (NWS) was treated in 200 mL of 1% CTAB at room temperature for 24 h in constant oscillator. Then, the sample was washed thoroughly with deionized water until neutralized and dried in the oven at 333 K. The natural wheat straw (NWS) and modified wheat straw (MWS) were characterized by FTIR and XRF. Then, MWS surface was used as adsorbent for the removal of methyl orange from aqueous solution. The studies were conducted under a variety of conditions that include temperature, contact time, pH, MWS dosage, and initial MO concentration. As the adsorbent dose of MWS rises, the adsorption capability of azo dye falls. Hence, the test employed 1.00 g/L as the dosage of MWS adsorbent for MO biosorption. At pH 3, MWS was more effective at adsorbing azo dye, but at lower and higher pH levels, the ability for biosorption was reduced. The biosorption capacity will rise when salt concentration rises up to 0.05 mol/L. The capacity of the equilibrium MWS decreases when temperature rises from 303 to 323 K. Three isotherm models (Langmuir, Freundlich and Temkin) were applied to study the equilibrium adsorption capacity of MO onto MWS. The equilibrium data are well described by the Freundlich model, which suggests that the biosorption process might involve many layers and/or surface heterogeneity of the adsorbent. As the contact time increased until equilibrium, the biosorption capacity rose accordingly. Therefore, the duration of 520 min was chosen as the best condition for additional studies. MWS adsorption capacity is 50.4 mg g^{-1} at 303 K under the optimum condition at pH 3, MWS dosage of 1.00 g L^{-1} and contact time of 520 min. The kinetic study was well described by the Elovich, PSO and intraparticle diffusion models. The results showed that the two essential elements of the adsorption process are film diffusion and intraparticle diffusion. This provided more evidence of the chemisorption process. Thermodynamic parameters $\Delta G°$, $\Delta H°$, and $\Delta S°$ were calculated, where negative values of $\Delta G°$ and $\Delta H°$ revealed the spontaneity, feasibility and exothermic biosorption process. A positive value of $\Delta S°$ suggested the increase in randomness at the solid–solution interface during the biosorption of MO onto MWS. The best desorption method for MO-loaded MWS was treatment with heated water that resulted in a desorption efficiency of 83.28%. In a related study, Mohamed et al. (2020) developed a series of chitosan-wheat straw biocomposites

that display tunable adsorption. The biocomposite pellets were evaluated under equilibrium and kinetic conditions to characterize the adsorption properties of anionic dyes (fluorescein and reactive black). An incremental dye adsorption affinity was noted for the biocomposite pellets with the anionic dyes in variable charge states, along with greater dye adsorption as the biomass content (wt %) increases. The study reported by Mohamed et al. (2020) highlights a *first-example* of a low-cost, facile, and sustainable approach for the utilization of such straw-chitosan composites which have promising potential for sorption-based dye removal from aqueous media.

The removal of the azo dye MO from aqueous media was studied (Tchuifon et al. 2014) with the use of two types of biosorbents, rice husk and egussi peeling at room temperature. A number of factors were tested that include contact time, adsorbent mass, pH, and initial dye concentration. The capacity of the adsorbents for adsorption increased along with the dye concentration and dose of the bio-sorbent. Both adsorbent surfaces revealed the highest levels of adsorption occur at pH 2, where the MO dye removal (%) are given for each system: egussi peeling (69.45%) and rice husk (70.31%,), where an initial MO concentration of 35 mg/L, adsorbent mass of 1.3 g, and a contact period of 10 min was employed. The kinetic models used for the study of the MO adsorption system by egussi peeling and rice husk include the following: PFO, PSO, Elovich model, intra-particle diffusion, intra-particle diffusivity and mass transfer. The results showed that the kinetic data were followed by the PSO kinetic model with correlation coefficients (R^2) values of 0.990 for rice husk and 0.992 for egussi peeling, which supported that chemisorption was the rate determining step. The isotherm analysis also showed that the Freundlich isotherm provided a good fit for rice husk and that the Langmuir model fit well for the adsorption by egussi peeling. These findings demonstrate the effectiveness of rice husk and egussi peeling as adsorbent surfaces for the removal of MO from aqueous media.

In 2014, Karimulla and Ravindhranath (2014) assessed the efficacy of thermally activated powders derived from the leaves, stems, and ashes of Thespesia populnea and Pongamia pinnata plants to remove MO dye from contaminated water. Different parameters such as the pH of solution, equilibrium time and sorbent dosage were studied to reveal maximum dye removal. The adsorption of MO was found to be sensitive to pH around 3, and greater dye removal (%) occurs at longer contact times. The amount of MO dye removed by the Thespesia populnea plant materials at pH 3 was reported as follows: 92.0% at 60 min or above for the leaf powders, 96.7% at 45 min for leaves ashes, 94.0% at 45 min for the stem powder and 98.9% at 30 min for the ashes of stems. Similar results were reported for the biomaterials of Pongamia pinnata, where the removal (%) of MO at pH 3 was 86.2% at 60 min or more for leaf powders, 91.0% at 45 min for leaf ashes, and 98.0% at 30 min for stem ashes. As the adsorbent dosage increased, the MO dye removal (%) increased. In the case of Thespesia populnea, 1.0 g/500 mL for leaf powder, 0.75 g/500 mL for the ashes,

0.5 g/500 mL for stem powders and 0.25 g/500 mL for the ashes. According to study, the ideal adsorbent dosage for the Pongamia pinnata plant is 0.25 g/500 mL for the ashes, 0.25 g/500 mL for the powdered leaves, and 0.50 g/500 mL for the powdered stems.

Moringa peregrine plant (MPTA) was investigated by Bazrafshan et al. (2014) for its potential as a cheap adsorbent to remove an azo dye (MO) from aqueous solution. The influence of different operating factors was investigated: initial concentrations (10–150 mg L^{-1}), contact time (10–150 min), pH (2–11) and adsorbent dosage (1–13 g L^{-1}). 96% removal of methyl orange (50 mg L^{-1}) was obtained for an MPTA dose of 7 g L^{-1} after a 70 min contact time at an optimum pH of 2. To relate to the equilibrium characteristics of the adsorption Freundlich and Langmuir models, two adsorption isotherm models were used. The Langmuir isotherm provided an account of the equilibrium adsorption data of MO onto MPTA. Therefore, the MO dye was assumed to be adsorbed as a monolayer onto the active sites that are homogeneously distributed over the MPTA surface. By raising the temperatures from 293 K to 313 K, the removal effectiveness of MO increased. The thermodynamic parameters were also evaluated. The negative values of standard difference for the Gibbs free energy ($\Delta G°$) suggest the spontaneity of adsorption system. Further evidence that the adsorption process is more advantageous at higher temperatures comes from the decrease in negative magnitude of ($\Delta G°$) with a rise in temperature. Also, the positive magnitudes of enthalpy change ($\Delta H°$) and entropy change ($\Delta S°$) indicate that the process of adsorption is endothermic with greater randomness after the dye adsorption.

The removal of anionic MO dye from aqueous solution using thermally treated egg shell as an adsorbent was studied by Belay and Hayelom (2014). The eggshell was washed with tap water, dried at 105 °C for an hour in a convection oven, pulverized with a mortar and pestle, and then immersed in a 1:1 weight-to-volume solution of H_2SO_4 for a whole night to improve the adsorption efficiency. Different parameters were examined such as adsorbent dose, contact time, particle size of adsorbent and initial concentration. The maximum removal efficiency of egg shell was found to be 98.8% for 12.5 mg/L, 2 g adsorbent dosage, and 20 min contact time as shown in Figure 14. Because of the increase in surface area and the availability of more adsorption/active sites, the removal efficiency rises with the amount of adsorbent. The removal effectiveness of MO diminishes as adsorbent particle size and the initial azo dye concentrations increase. Due to the increased surface area, activated egg shell increased the removal (%) of acidic dye from aqueous solution. The egg shell is an appropriate adsorbent and has affinity to remove MO from aqueous media, according to the experimental findings of this study.

In 2015, study by Krika and Benlahbib (2015) used cork powder as an inorganic adsorbent for removal of MO from aqueous media. Batch operating conditions were used to study the effect of various factors on the MO adsorption such as contact time, initial concentrations, adsorbent dosage, solution pH, ionic strength and temperature. The
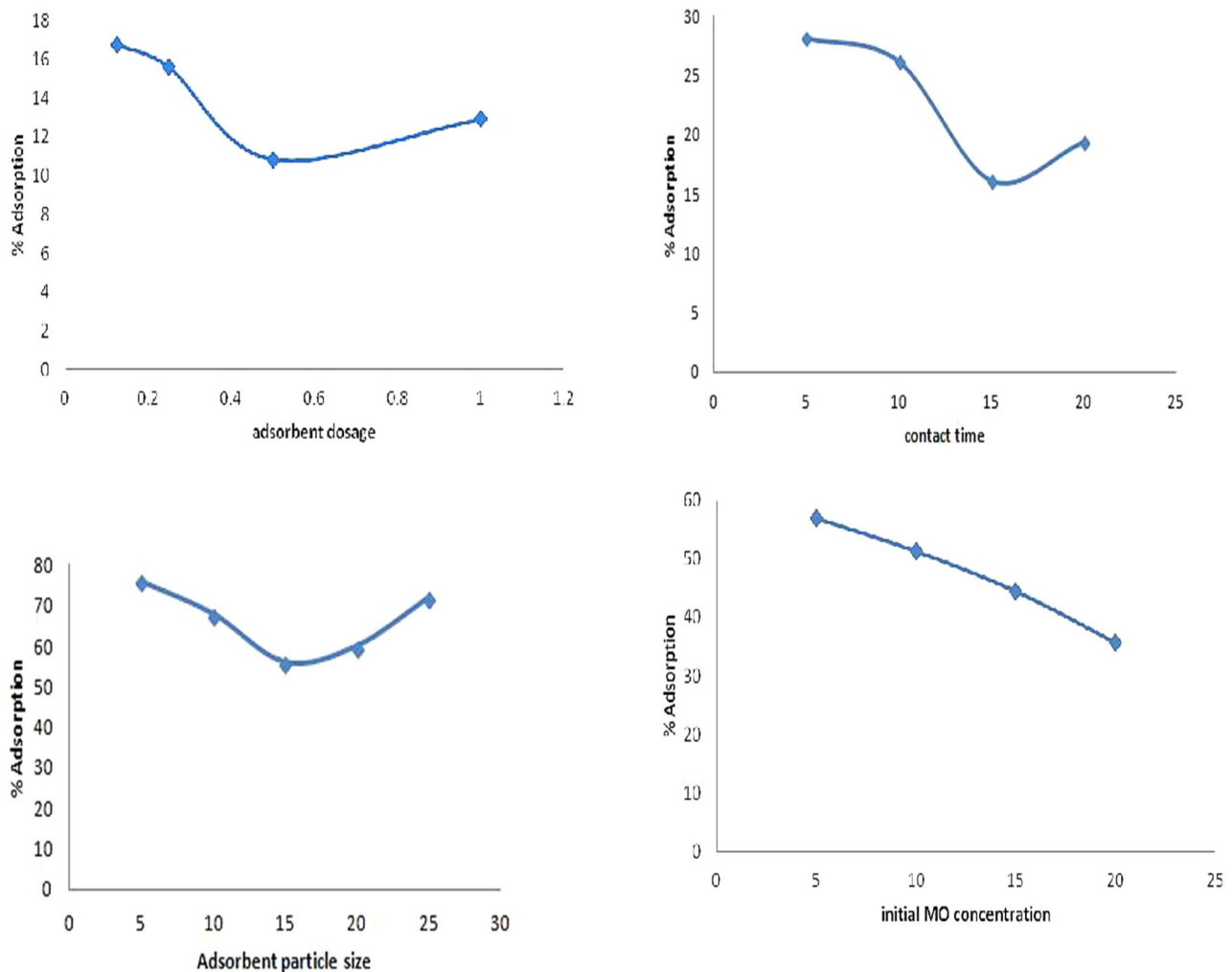
Figure 14. Percentage adsorption of MO dye as a function of various parameters: (A) Adsorbent dosage, (B) Contact time, and (C) Particle size of adsorbent, and (D) Initial MO concentration (Belay and Hayelom 2014).

properties of surface and structural effects of cork were characterized by various techniques: SEM, FT-IR, point of zero charge, and Boehm titration method. Maximum adsorption capacity of cork for MO is 16.66 mg g^{-1} at 298 K under the optimum solution condition at pH 2, cork mass of 5.00 g L^{-1}, particle size of $d < 0.08$ mm, and contact time of 240 min. The percentage of anionic or acidic dye removal falls as the pH solution, ionic strength, and adsorbent particle size rise, but rises when the adsorbent dosage rises from 1 to 5 g/L. The amount of the anionic dye adsorbed onto cork increased from 2.45 to 9.35 mg/g with an increase in the initial MO concentration (20 to 100 mg/L). The adsorption capacity declines with increasing temperatures. The adsorption capacities of cork were 5.02, 4.50, and 3.76 mg g^{-1} at 298, 308, and 318 K, respectively. Based on correlation coefficient ($R^2 = 0.99$), the equilibrium data were well described by the Langmuir isotherm. Moreover, the kinetic data indicate that the PSO model was the best applicable model to the experimental results. The value of standard Gibbs free energy of dye adsorption ($\Delta G°$) was found to be (-14.96 kJ/mol), the negative value proved the spontaneity of the MO adsorption system onto the cork surface. The values of ($\Delta H°$; -11.71 kJ/mol) and ($\Delta S°$;

-10.93 J/mol. K) were estimated for the adsorption of MO by cork, which suggests that the adsorption process was exothermic with decreased randomness.

The effectiveness of rice husk as an adsorbent for the adsorptive removal of methyl orange from aqueous solution was studied by Purbaningtias et al. (2015). The study highlighted several parameters such as pH, equilibrium time and initial dye concentration. The removal efficiency decreases as the pH of dye solution increases. The adsorption capacity increases with greater contact time and initial concentrations. The adsorption of MO was optimum at pH 3 with an optimum contact time in 7 h and an initial concentration of 230 mg/L. Adsorption of MO corresponds with the PSO model according to the favorable goodness-of-fit (R^2). The equilibrium dye adsorption was examined using the Langmuir and Freundlich isotherm models, where the results reveal that the Langmuir isotherm had the best fit for the MO adsorption onto rice husk with a maximum adsorption capacity of 243.9 mg/g.

Kamaru et al. (2016) examined the adsorption efficiency of pineapple leaf powder (PLP) and modified leaf powder treated with cationic surfactant (SMPLP) to enable removal of MO anionic dye from aqueous media at room

temperature. The surfactant-modified pineapple leaf powder (SMPLP) was prepared by mixing PLP with HDTMA-Br solution in the ratio of 10:1 (PLP: HDTMA-Br solution, w/v) under constant stirring for 15 min at room temperature. After filtering, the SMPLP was dried for 24 h at 90 °C. The unmodified and modified PLP were characterized by FTIR spectroscopy and SEM. Batch mode experiments were tested to demonstrate the effects of the initial adsorbate concentration, pH, temperature and surfactant concentrations on the adsorption quantity of PLP and SMPLP with MO dye system. As the starting concentration of the HDTMA-Br solution grew from 1.0 to 4.0 mM, the amount of HDTMA-Br adsorbed onto SMPLP increased from 138.6 to 381.7 mmol/kg. At pH 3, the adsorption of MO onto PLP and SMPLP was greater, and at pH 4, it rapidly decreased. The adsorption capacity was steady between pH values of 4 and 10, however it further dropped at pH 11. At pH 3.00, MO was more likely to be bound to the adsorbent with rising initial MO concentrations, PLP and SMPLP's ability to adsorb MO rose as well. The adsorption capacity of PLP and SMPLP decreased as the temperature rose from 308.15 to 333.15 K. The adsorption data were well fitted into the Langmuir isotherm model with maximum monolayer adsorption capacity for MO of 47.61 mg/g. The negative values for ($\Delta G°$, $\Delta H°$, and $\Delta S°$) for the adsorption process at all temperatures indicate the spontaneous nature of the process, exothermic nature and decrease in the randomness at the solid/solution interface.

In order to increase the capacity of a commercial coffee waste (CW) to adsorb MO from aqueous media (Lafi and Hafiane 2016) treated the CW with cationic surfactants CTAB or cetylpyridinium chloride (CPC). The organo – CW was prepared by mixing 2.5 g of CW with 0.5 L of 0.027 mol/L surfactant solutions, and then the mixtures were agitated in a shaker device at 220 rpm and 25 ± 1 °C for 48 h. The unmodified surface (CW) and modified surface (MCWs) were characterized using FTIR spectroscopy. Various factors such as pH, contact time, adsorbent dosage and salt effect were examined. For CTAB-CW and CPC-CW, an increase in adsorbent dosage from 0.2 to 20 g/L resulted in an increase in the percentage of dye removal from 41.1 to 99.3 and from 37.9 to 98.5, respectively. As the pH increased from 2.9 to 10.3, the adsorption capacity decreased from 23.48 mg/g to 7.06 mg/g for CTAB-CW and from 23.64 mg/g to 8.11 mg/g for CPC-CW. The maximum dye adsorption onto the modified commercial coffee waste (MCWs) was revealed at pH 3.5 with 0.1 g/50 mL of adsorbent. The adsorption capacity dropped marginally from 22.6 to 21.8 mg/g for CTAB-CW and from 22.2 to 21.1 mg/g for CPC-CW when the salt (NaCl) concentration rose from 0 to 10 g/L. This trend indicates that the influence of ionic strength was modest as noted in Figure 15. The Langmuir isotherm model provided better fit to the experimental data, which depends on monolayer adsorption onto the adsorbent surface. The maximum adsorption capacities of MCWs for dye at 25 °C for CTAB-CW is 58.82 and for CPC-CW is 62.5 mg/g. The adsorption mechanism showed better agreement with the PSO kinetic model based on the correlation
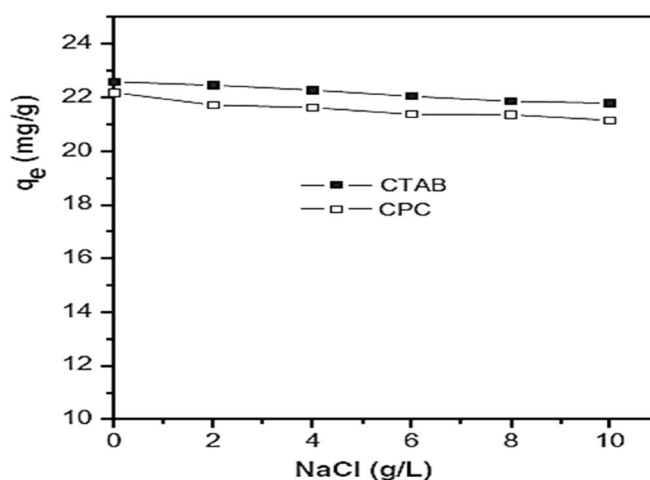

Figure 15. Effect of ionic strength on the adsorption of MO on CTAB-CW and CPC-CW (Lafi and Hafiane 2016).

coefficients (R^2, 0.99). Thermodynamic studies were carried out at various temperatures (298, 308, 318 and 328 K). The process was thermodynamically spontaneous based on the negative values of ($\Delta G°$) in the ranges of −7.80 to −7.64 for CW-CTAB and −8.62 to −8.34 kJ/mol for CW-CPC. The fact that ($\Delta H°$) is negative for CW-CTAB (−9.38 kJ/mol) and CW-CPC (−11.39 kJ/mol) supports the exothermic nature of the adsorption process. The value of entropy $\Delta S°$ is negative (−0.005 kJ/mol and −0.009 kJ/mol) for CW-CTAB and CW-CPC, respectively, due to decreased randomness for the dye adsorption process onto the surface of the adsorbents. More recently, Steiger et al. (2021) prepared biosorbents that contain spent coffee grounds (SCG) that were shown to have relatively high adsorption capacity toward a cationic dye (methylene blue; MB), where the adsorption capacity with MB ranged from 18 to 98 mg/g for the SCG adsorbents (without cross-linking) to ca. 135 mg/g for the cross-linked SCG adsorbents.

Amine modified pumpkin seed powder (APSP) was studied by Subbaiah and Kim (2016) as a potential adsorbent for the removal of MO from aqueous media. For the preparation of APSP, 5 g of the sample was suspended in 100 mL of ethanolamine, and 20.8 mL of concentrated HCl was added to the suspension. The mixture was agitated on a rotary shaker at 150 rpm for 6 h. Batch adsorption experiments were studied to account for the role of contact time, pH and temperature. The APSP surface was analyzed by different methods that include FTIR and SEM. The amount of adsorption decreases from 126.1 to 4.9 mg/g as the pH increases from 3 to 11. As the equilibrium time increases, the MO dye adsorption increases. Therefore, a fixed time (110 min) was used as the equilibrium time in all adsorption experiments. By increasing the temperature from 298 to 313 K, the amount of adsorbed dye with APSP increased from 143.7 to 200.3 mg/g. The experimental equilibrium studies were evaluated using several isotherm models (Langmuir, Freundlich, Sips and Toth). The adsorption results were best described by the Langmuir and Sips isotherms. The maximum monolayer adsorption capacity was found to be 200.3 mg/g according to the Langmuir isotherm

model. The kinetic data was well represented by the PSO kinetic model ($R^2 < 0.97$). The thermodynamic parameters such as (ΔG^0, negative) proved that the adsorption of MO onto APSP was energetically favorable and spontaneous in the temperature range 298–318K. Whereas, the terms for (ΔH° and ΔS^0) are positive, which indicate that the process is endothermic with greater randomness at the solid-solution interface upon adsorption of MO onto the active site of the APSP. The experimental results indicated that APSP may serve as a potential adsorbent for MO removal from aqueous media.

A study by Eljiedi and Kamari (2017) used the shell of lala clam's (Orbicularia orbiculata) as a cheap adsorbent to remove MO from aqueous media. The biomass surface was analyzed using Field Emission Scanning Electron Microscope (FESEM) and FTIR spectroscopy. The adsorption process is influenced by several variables: pH, initial dye concentration and adsorbent dosage. A rise in pH led to decreased adsorption of MO, while an initial rise in the concentration of MO dye (2.5–20 mg L^{-1}) increased the effectiveness of MO removal by lala clam shells. The maximum removal (%) of MO was 18.9%, where greater adsorption of the dye occurred with decreasing dosage of adsorbent from 2.5 to 0.1 mg/g. The adsorption system was optimal at pH 2.0 and an initial anionic dye concentration of 20 mg/L. Two isotherm models (Freundlich and Langmuir) were applied to analyze the equilibrium parameters, where the Freundlich isotherm model provided the best-fit. This trend suggests that the heterogeneous nature of the adsorbent surface and the potential benefits of the lala clam shell for removal of the anion form of MO dye from aqueous media.

Fadhil and Eisa (2019) investigated a comparative study between non-activated and activated corn leaves with 0.1% vol. HCl for 24 h as an adsorbent material for the adsorption of the hazardous MO dye. FTIR spectroscopy and SEM were employed to characterize the adsorbent. The effect of different variables (contact time, amount of adsorbent, initial dye concentration, temperature and pH) on the dye removal efficiency were tested. The results reveal that the adsorption efficiency rises to 71% and 93% with greater dye concentration for non-activated and activated corn leaves, respectively. For both adsorbent materials, the proportion of dye removal rises as adsorbent weight increases. The amount of adsorption and the dye removal (%) increase with passing time until equilibrium is reached at day 4 for treated and untreated surfaces. For non-activated and activated maize leaves, respectively, the removal efficiency decreased from 78.2% to 49.5% and from 85% to 55% as the pH of the solution increased. As the temperature increases, the adsorption capacity decreases for both activated and non-activated adsorbents. The equilibrium study is best represented by the Freundlich isotherm for non-activated corn leaves, while the Langmuir isotherm shows better agreement with the experimental result for activated corn leaves. The adsorption rate was obeyed by the PFO kinetic model for untreated corn leaves, while the PSO model accounted for the kinetic results for the treated corn leaves as revealed in Figure 16.
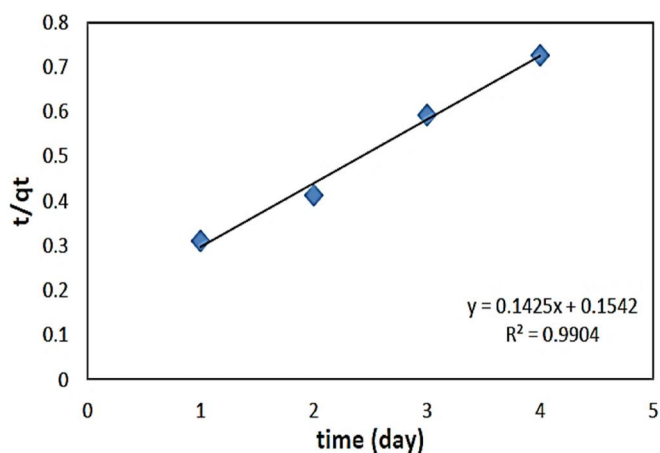

Figure 16. A pseudo-second order (PSO) kinetic plot of MO adsorption by activated corn leaf (Fadhil and Eisa 2019).

El Maguana et al. (2020) used sugar scum powder as an effective and affordable adsorbent to remove MO from aqueous solution. Utilizing several complementary methods (XRD, SEM/EDX, FTIR spectroscopy, and SEM coupled with energy dispersive X-ray spectroscopy), the properties of the adsorbent were characterized. The effects of different parameters including initial concentration, contact time, and adsorbent dosage were studied. As the initial concentration of the dye solution was raised, more adsorption occurred. Greater adsorption occurs as the process proceeds until equilibrium is established after 60 min. An increasing dosage of sugar scum powder (1 to 16 g/L) results in greater removal of MO until it reaches its maximum removal effectiveness of 80% at 16 g/L. The adsorption system followed the PSO kinetic and Langmuir adsorption isotherm models. The maximum monolayer adsorption capacity for the anionic form of MO dye was 15.24 mg/g at 22 °C and pH 7.2. The standard difference in thermodynamic parameters ΔG°, ΔH° and ΔS° for the adsorption process were investigated. Negative values of ΔG° and ΔH° suggest the feasibility and exothermic nature of the physical adsorption process onto sugar scum powder for all temperatures (293, 303 and 318). The positive value of ΔS° reveals a greater randomness at the solid-solution interface during the MO adsorption process. The experimental studies suggested that sugar scum is a suitable adsorbent for MO dye removal from wastewater.

The green shell (Perna Viridis), a natural substance was tested by Fajarwati et al. (2020), to absorb the anionic form of MO dye. At 200 mesh, the chosen adsorbent was sieved prior to characterization and adsorption studies. SEM-EDX was used to characterize the adsorbent via its composition and morphology, which revealed a homogeneous adsorbent surface. The optimum MO adsorption capacity occurred at an activation temperature of 900 °C (adsorption (%) = 39.06%) with 1.5 g of adsorbent (adsorption (%) = 94.65% at pH 10 (% adsorption of 21.68%) and at contact time of 45 min (% adsorption of 98.67%). Adsorption kinetics of MO onto green shell was followed by the PSO model.

Shah et al. (2021) investigated the feasibility of utilizing the leaves of populous tree (PPLS) in five different forms

(PPLSD, PPLSCHR, PPLSACD, PPLSACCHR and PPLSLARG) for the adsorption of MO dye from aqueous media. The PPLS was cleaned with tap water, allowed to dry in the sun, and then crushed. The dusty and crushed material was cleaned with deionized water before drying for 30 h at 70 °C. In order to obtain populous leaves charcoal (PPLSCHR), populous leaves dust was kept in a muffle furnace at 700 °C in a nitrogen atmosphere for 1 h. For impregnation of PPLSD with acetic acid, 10 g of PPLSD was treated with 500 mL of 1 M aqueous acetic acid solution was heated at 50 °C for 60 min. The solution was decanted and acid impregnated dust was treated with 500 mL of 0.3 M HCl aqueous solution, followed by stirring for 3 h at 50 °C. The wet residue was kept in an oven at 100 °C until dried to obtain protonated acetic acid impregnated populous dust (PPLSACD). Similarly, 10 g of PPLSCHR was treated with 500 mL of 0.034 mL-arginine aqueous solution and the above process was used to obtain protonated L-arginine impregnated populous charcoal (PPLSLARG). The physicochemical properties of all adsorbents were characterized using FTIR spectroscopy, XRD, SEM and Brunauer-Emmett-Teller (BET) analysis. The effect of varying parameters such as adsorbent mass, pH, initial concentration, and contact time were examined. From pH 3 to 12, the effectiveness of dye removal for all adsorbents declined. The adsorption capability of each adsorbent rose with the initial dye concentration (5 ppm to 75 ppm) and as the adsorbent mass rose from 0.2 g to 0.6 g. The Langmuir and Freundlich isotherm models were used to fit the dye adsorption profiles on all adsorbent surfaces. The outcomes reveal that the Langmuir isotherm was a good fit for the MO dye adsorption with the various adsorbents. The maximum monolayer adsorption capacity was found to be 90.44 mg/g at pH 3.0 and 303.15 K with a fovourable coefficient of determination (R^2, 0.9988) for PPLSLARG. The kinetic data indicated that the system followed the PFO kinetic model for all of the adsorbents, where a satisfactory coefficient of determination ($R^2 > 0.93$) was obtained. The thermodynamic parameters $\Delta G°$, $\Delta H°$ and $\Delta S°$ were estimated, where positive values of $\Delta G°$ and $\Delta S°$ indicated that the adsorption phenomenon of MO moved toward non spontaneity at all adsorbent surfaces and the degree of freedom increased after the dye adsorption onto the adsorbents. While the negative value of $\Delta H°$ for all adsorbents implied that the adsorption process was exothermic in nature. Using quadratic models and optimizing the conditions, the maximum adsorption capacity for all the adsorbents was observed at an initial concentration 75 ppm, adsorbents mass 0.6 g and pH 5.

Coal fly ash, a readily available and inexpensive adsorbent for the elimination of MO that was examined by Potgieter et al. (2021). The adsorption studies for anionic dye removal were tested under various conditions such as batch, column and heap adsorption at variable temperature and adsorbent dosages at neutral pH. The dye removal efficiency increased with temperature from 20 °C to 40 °C. The Langmuir, Freundlich and Temkin isotherm models were applied to determine the best-fit to the equilibrium profiles for the systems. The Freundlich model described the equilibrium
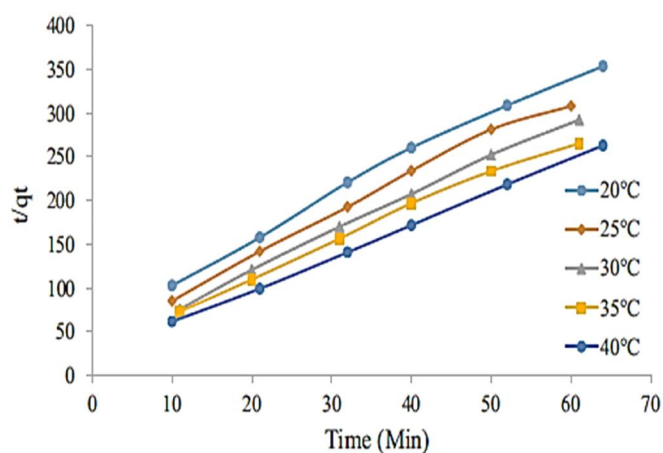

Figure 17. Lagergren pseudo-second order (PSO) plot for the adsorption of MO at various temperatures (Potgieter et al. 2021).

process, whereas the PSO model accounted for the adsorption kinetics, as seen in Figure 17. Upon study of the thermodynamic parameters, negative values for the Gibbs free energy change $\Delta G°$ prove the process is spontaneous. A positive change for $\Delta H°$ and $\Delta S°$ suggest that the adsorption process is endothermic, random and physical in nature. The negative value of activation energy suggesting that energy barriers are negligible. The column configuration was found to be the most effective for the dye removal efficiency of 99.95%, followed by heap adsorption at 99.25% removal, whereas batch adsorption resulted in 96.68% removal. Dye adsorption was highest using a column-based system. Table 4 lists the effectiveness of the various adsorbent substances, including both modified and unmodified bio-sorbents employed for removal of MO from aqueous media. Table 5 lists the kinetic parameters of PFO and PSO models, along with the thermodynamic parameters for adsorption of MO dye onto the modified and unmodified bio-sorbents.

Group C: Biochar

Biochar is considered as the solid carbonaceous product of biomass obtained via pyrolysis at a lower temperature, typically less than 700 °C under anaerobic conditions. Biochar is a common adsorbent due to its surface area, enriched surface functional groups, relatively low cost and high-adsorption capacity. Eco-friendly biomass wastes such as agricultural waste, manure, and forestry waste have been used for the removal of MO from aqueous media (Yu et al. 2018; Iwuozor et al. 2021).

Yu et al. (2018) studied the capability of the biochar adsorbent carboxymethyl cellulose (CMC), which was derived from the pyrolysis (600 °C, 120 min and under N_2 gas at 200 mL·min^{-1}) of chicken manure for the removal of the anionic MO dye from aqueous solution. The physicochemical properties of adsorbent material before and after pyrolysis were analyzed by SEM and FTIR spectroscopy. The experimental factors including agitation speed, pH, adsorbent dose and contact time were examined. As the agitation speed was increased from 50 rpm to 250 rpm, the removal (%) of MO increased, where the optimum agitation

Table 4. Adsorption performance of MO by Group B adsorbents.

Adsorbent name	q_{max} (mg/g)	pH	Temp (°C)	Model for q_{max} determination	Reference
Kudzu starch	0.78	–	30	Langmuir Freundlich	(Boki et al. 1991)
Sweet potato	1.20	–	30	Langmuir Freundlich	(Boki et al. 1991)
Corn starch	1.63	–	30	Langmuir Freundlich	(Boki et al. 1991)
Rice starch	1.25	–	30	Langmuir Freundlich	(Boki et al. 1991)
Wheat starch	2.03	–	30	Langmuir Freundlich	(Boki et al. 1991)
Potato starch	0.00	–	30	Langmuir Freundlich	(Boki et al. 1991)
Snake gourd starches	0.00	–	30	Langmuir Freundlich	(Boki et al. 1991)
Orange peel	20.50	7	30	Langmuir	(Annadurai et al. 2002)
Banana peel	21.50	7	30	Langmuir	(Annadurai et al. 2002)
Bottom ash	10.72	3	50	Freundlich	(Mittal et al. 2007)
De-oiled soya	1.75	3	50	Langmuir	(Mittal et al. 2007)
Boiler fly ash	499.79	–	–	Freundlich	(Okoronkwo et al. 2008)
Skin almonds	1.51	–	23	Freundlich	(Atmani et al. 2010)
Prunus amygdalus L. (almond) shell	41.34	3	20	Langmuir	(Deniz 2013)
Dragon fruit foliage	9.76	6	55	Freundlich	(Haddadian et al. 2013)
Cetyl trimethyl ammonium bromide modified wheat straw	50.4	3	30	Freundlich	(Su et al. 2014)
Egussi peeling	13.89	2	–	Langmuir	(Tchuifon et al. 2014)
Rice husk	1.917×10^{-2}	2	–	Freundlich	(Tchuifon et al. 2014)
Thermally powder from leaves, stems and their ashes of Thespesia populnea and Pongamia pinnata plants	–	3	–	–	(Karimulla and Ravindhranath 2014)
Thermally treated egg shell	–	–	–	–	(Belay and Hayelom ,2014)
Moringa peregrine plant	15.78	2	30	Langmuir	(Bazrafshan et al. 2014)
Cork powder	16.66	2	25	Langmuir	(Krika and Benlahbib 2015)
Rice husk	243.90	3	–	Langmuir	(Purbaningtias et al. 2015)
Pineapple leaf	47.60	3	–	Langmuir	(Kamaru et al. 2016)
Hexadecyltrimethylammonium bromide modified pineapple leaf	47.61	3	–	Langmuir	(Kamaru et al. 2016)
CTAB or CPC modified coffee waste	62.50	3.5	25	Langmuir	(Lafi and Hafiane 2016)
Aminated pumpkin seed	200.30	–	45	Langmuir	(Subbaiah and Kim 2016)
Lala clam (Orbicularia orbiculata) shel	0.0008	2	–	Freundlich	(Eljiedi and Kamari 2017)
Corn leaves	0.24	–	30	Freundlich	(Fadhil and Eisa 2019)
HCl modified corn leaves	4.93	–	30	Langmuir	(Fadhil and Eisa 2019)
Sugar scum	15.24	7.2	22	Langmuir	(El Maguana et al. 2020)
Green shell (Perna Viridis)	–	10	900	–	(Fajarwati et al. 2020)
Populous leaves dust	39.85	3	30	Langmuir	(Shah et al. 2021)
Populous leaves charcoal	44.08	3	30	Langmuir	(Shah et al. 2021)
Acetic acid impregnated populous dust	53.18	3	30	Langmuir	(Shah et al. 2021)
Acetic acid impregnated populous charcoal	65.62	3	30	Langmuir	(Shah et al. 2021)
L-arginine impregnated populous charcoal	90.44	3	30	Langmuir	(Shah et al. 2021)
Coal fly ash	0.42	–	22	Freundlich	(Potgieter et al. 2021)

speed (150 rpm) was chosen for the batch experiments. As the pH was changed from 5.5 to 8.5, the adsorption decreased from 22.30 mg/g to 20.42 mg/g. Therefore, the initial pH of 6.5 was selected as the optimal value. An increase of the dosage of CMC from 0.2 g/L to 1.4 g/L led to greater MO removal efficiency from 29.37% to 100%. Consequently, the optimal adsorbent dosage was chosen as 1.0 g/L. The kinetic studies of different initial concentration were well described by the PSO model as revealed in Figure 18. The Langmuir isotherm model provided a better fit with the equilibrium data ($R^2 > 0.99$), where a maximum adsorption capacity (39.47 mg.g^{-1}) was determined at 25 °C. The thermodynamic parameters $\Delta G°$, $\Delta H°$ and $\Delta S°$ were calculated at 25 °C, 35 °C and 45 °C. The negative values of $\Delta G°$ revealed that the MO was adsorbed by CMC in a practical and spontaneous manner. Positive values of $\Delta H°$ and $\Delta S°$ were obtained, indicating that the adsorption process was endothermic with greater disorder at the solid/solution interface during the adsorption of MO onto CMC The experimental results of this study suggested that CMC is an effective adsorbent for decontamination of dyes from aqueous media. Two types of biochar were utilized to remove MO from aqueous solutions that are listed in Table 6. Kinetic parameters were obtained by the PFO and PSO models, along with the thermodynamic parameters for adsorption of MO dye by the biochar systems listed in Table 7.

Group D: Activated carbon

A carbonaceous material known as activated carbon (AC) is created by heating carbon-rich organic materials, including charcoal, coconut shells, wood, coal, and inorganic materials such as egg shells, to extremely high temperatures exceeding

Table 5. Kinetic parameters of pseudo-first order (PFO), pseudo-second order (PSO) models and thermodynamic parameters for adsorption of MO dye by Group B adsorbents.

Adsorbent name	K_1 (min^{-1})	K_2 (g/mg min)	Temp. (°C)	$\Delta H°$ (kJ mol^{-1})	$\Delta G°$ (kJ mol^{-1})	$\Delta S°$ (J mol^{-1} K^{-1})	(Ref.)
Kudzu starch	–	–	–	–	–	–	(Boki et al. 1991)
Sweet potato	–	–	–	–	–	–	(Boki et al. 1991)
Corn starch	–	–	–	–	–	–	(Boki et al. 1991)
Rice starch	–	–	–	–	–	–	(Boki et al. 1991)
Wheat starch	–	–	–	–	–	–	(Boki et al. 1991)
Potato starch	–	–	–	–	–	–	(Boki et al. 1991)
Snake gourd starches	–	–	–	–	–	–	(Boki et al. 1991)
Orange peel	0.40	–	30	–	–	–	(Annadurai et al. 2002)
Banana peel	0.39	–	30	–	–	–	(Annadurai et al. 2002)
Bottom ash	0.06	–	30	−16.76	−25.77	30.69	(Mittal et al. 2007)
De-oiled soya	0.03	–	30	−4.79	−24.74	58.21	(Mittal et al. 2007)
Boiler fly ash	4.60×10^{-6}	1×10^5	–	–	–	–	(Okoronkwo et al. 2008)
Skin almonds	–	0.03	23	–	–	–	(Atmani et al. 2010)
Prunus amygdalus L. (almond) shell	0.91	12.70	20	−16.86	−6.54	−0.03	(Deniz 2013)
Dragon fruit foliage	–	14.3×10^{-3}	25	61.71	−0.25	208.00	(Haddadian et al. 2013)
CTAB modified wheat straw	0.07	5.41×10^{-3}	30	−0.49	−9.21	32.00	(Su et al. 2014)
Egussi peeling	0.16	2.23	–	–	–	–	(Tchuifon et al. 2014)
Rice husk	0.03	3.31	–	–	–	–	(Tchuifon et al. 2014)
Thermally powder from leaves, stems and their ashes of Thespesia populnea and Pongamia pinnata plants	–	–	–	–	–	–	(Karimulla and Ravindhranath 2014)
Thermally treated egg shell	–	–	–	–	–	–	(Belay and Hayelom 2014)
Moringa peregrine plant	–	–	20	43.13	2.17	140.00	(Bazrafshan et al. 2014)
Cork powder	0.06	0.01	25	−11.71	−14.96	−10.93	(Krika and Benlahbib 2015)
Rice husk	4.12×10^{-1}	7.53×10^{-7}	–	–	–	–	(Purbaningtias et al. 2015)
Pineapple leaf	–	–	–	–	–	–	(Kamaru et al. 2016)
Hexadecyltrimethylammonium bromide modified pineapple leaf	–	–	35	−8.74	−3.74	−0.01	(Kamaru et al. 2016)
CTAB or CPC modified coffee waste	0.02	0.003	25	−9.38	−7.80	−0.005	(Lafi and Hafiane 2016)
Aminated pumpkin seed	0.15	0.002	25	33.37	−2.76	123.00	(Subbaiah and Kim 2016)
Lala clam (Orbicularia orbiculata) shel	–	–	–	–	–	–	(Eljiedi and Kamari 2017)
Corn leaves	3.22	−0.14	30	–	–	–	(Fadhil and Eisa 2019)
HCl modified corn leaves	0.82	0.92	30	–	–	–	(Fadhil and Eisa 2019)
Sugar scum	0.11	0.005	20	−14.14	−14.63	2.03	(El Maguana et al. 2020)
Green shell (Perna Viridis)	9.90×10^{-6}	0.55	–	–	–	–	(Fajarwati et al. 2020)
Populous leaves dust	0.05	0.002	30.15	–	–	–	(Shah et al. 2021)
Populous leaves charcoal	0.04	0.001	30.15	–	–	–	(Shah et al. 2021)
Acetic acid impregnated populous dust	0.05	0.002	30.15	–	–	–	(Shah et al. 2021)
Acetic acid impregnated populous charcoal	0.05	0.001	30.15	–	–	–	(Shah et al. 2021)
L-arginine impregnated populous charcoal	0.05	0.001	30.15	–	–	–	(Shah et al. 2021)
Coal fly ash	0.01	0.33	20	13.36	−9.36	77.75	(Potgieter et al. 2021)

700 °C with activated gas (Sultana et al. 2022). Because of its porous structure, extremely large surface area (500 to 3000 m^2/g), microporous nature, thermal stability, and reactivity, activated carbon is frequently used for MO adsorption (Iwuozor et al. 2021).

Coconut shell fibers were utilized by (Singh et al. 2003) to prepare AC for the removal of acidic dye, MO, from wastewater. The coconut fibers were treated with concentrated sulfuric acid, and the same was kept in an oven maintained at 150–165 °C for a period of 24 h. Then, the carbonized material was subjected to thermal activation at different temperatures, viz., 200, 400, 600, and 800 °C for 1 h. The adsorption parameters were performed at different temperatures, particle size, pH, and adsorbent dose. For pH values between 2 and 4, a dramatic drop in the adsorption (%) of MO was noted. Consequently, pH 4 was selected as the ideal value for all of the adsorption studies on MO dye. With larger adsorbent particles, the absorption of MO dye on the produced AC declines. When the adsorbent dose is increased from 5 to 10 g/L, the removal efficiency of MO increases from 26 to 56%. Therefore, the dose of AC was held constant at 2.0 g/L throughout the adsorption trials, where temperatures between 30 °C and 50 °C resulted in greater dye adsorption. The Freundlich isotherm had better agreement with the experimental results versus the Langmuir isotherm, according to the best-fit parameters. The maximum adsorption capacity of MO onto AC derived from coconut shell fibers was 2.88×10^{-5} mol/g. The kinetic studies were also conducted, and the adsorption of MO followed the PFO kinetics model. To support the adsorption mechanisms, various kinetic parameters such as the mass-transfer coefficient, diffusion coefficient, activation energy, and entropy of activation were investigated. MO is adsorbed through particle diffusion at high concentrations and film diffusion at low concentrations.

Samarghandi et al. (2009) investigated the adsorption of MO from aqueous solutions onto AC derived from granular pine cone (GPAC). In all of the adsorption studies the dose of GPAC was kept at (0.05 g), initial dye concentration (100 mg/L), pH at 7.5 ± 0.2 and contact time of (370 min) at 20.3 °C. Several isotherm equations were used fit the experimental data (Langmuir, Freundlich, Dubinin-Radushkevic, Temkin, Halsey, Jovanovic and Hurkins-Jura). The fitting results showed that the data were best described by the
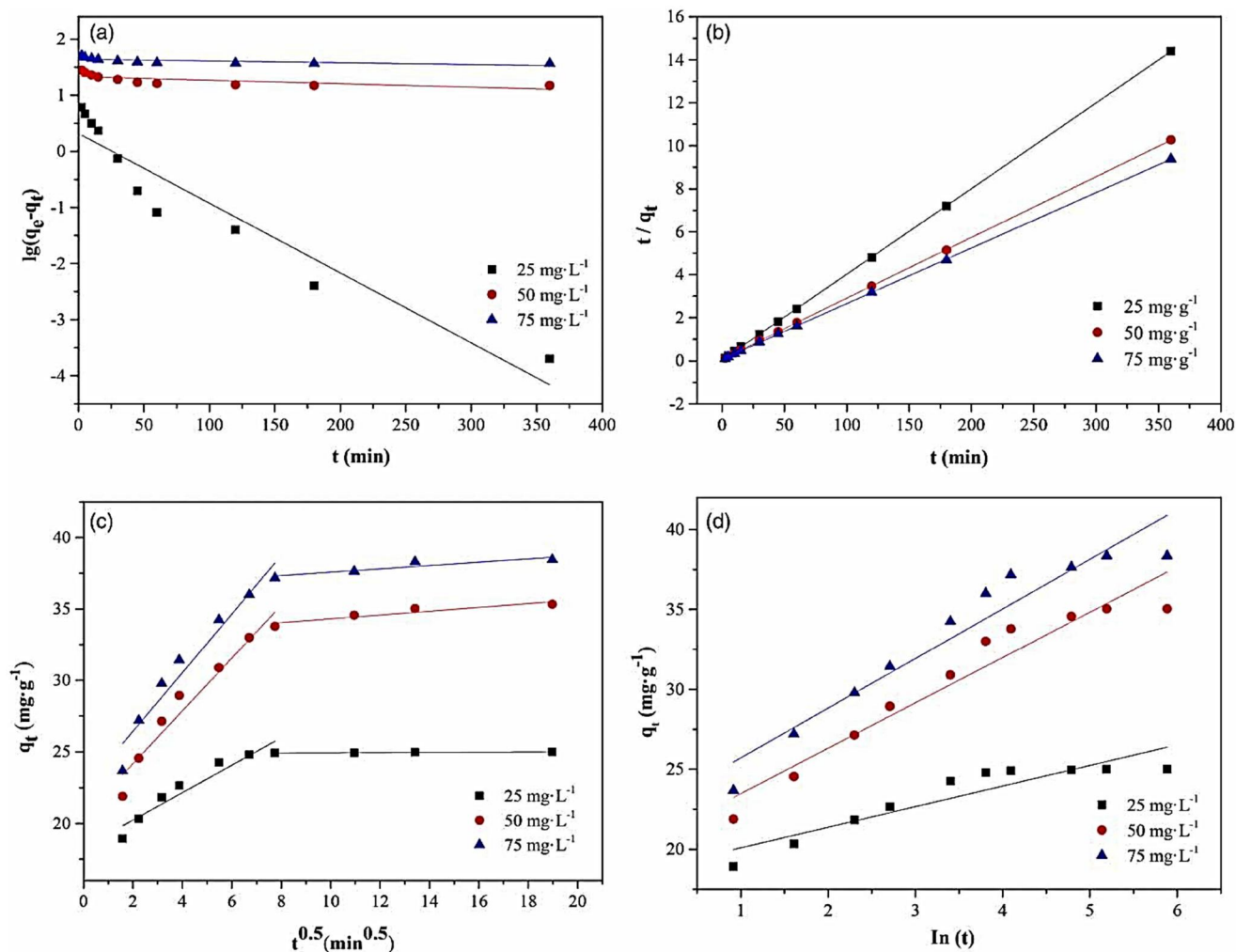
Figure 18. Kinetic fits for MO adsorption on CMC using different models: (a) pseudo-first-order (PFO); (b) pseudo-second order (PSO); (c) intra-particle diffusion; and (d) Elovich models (Yu *et al.* 2018).

Table 6. Adsorption performance of MO by Group C adsorbents.

Adsorbent name	q_{max} (mg/g)	pH	Temp (°C)	Model for q_{max} determination	Reference
Biochar from pulp and paper sludge	22.0	8	25	Freundlich	(Chaukura *et al.* 2017)
Biochar from chicken manure	39.47	–	25	Langmuir	(Yu *et al.* 2018)

Table 7. Kinetic parameters of pseudo-first order, pseudo-second order models and thermodynamic parameters for adsorption of MO dye by Group C adsorbents.

Adsorbent name	k_1 (min^{-1})	k_2 (g/mg min)	Temp. (°C)	$\Delta H°$ (kJ mol^{-1})	$\Delta G°$ (kJ mol^{-1})	$\Delta S°$ (J mol^{-1} K^{-1})	Reference
Biochar from pulp and paper sludge	0.03	32.50	25	–	−5.93	–	(Chaukura *et al.* 2017)
Biochar from chicken manure	0.02	0.04	25	7.55	32.94	−2.24	(Yu *et al.* 2018)

adsorption isotherm models in descending order of agreement: Langmuir > Jovanovic > Dubinin-Radushkevic > Temkin > Freundlich > Halsey > Hurkins-Jura models. The maximum monolayer adsorption capacity of GPAC with MO was 404.42 mg/g (cf. Figure 19). A comparison of various kinetic models (PFO, PSO, Elovich and Lagergren) reveals that the kinetic profiles obeyed the PFO kinetic model with low Chi-square values ($\chi^2 = 9.231$).

Chen S *et al.* (2010) investigated how AC prepared from Phragmites australis (PAAC) could remove MO from aqueous media. The adsorption and desorption isotherms of N_2

at 77 K for the PAAC sample are clearly type IV, according to the IUPAC classification. The PAAC surface is a high-quality adsorbent with a surface area of 1362 m^2/g. The pore volume is 1.271 cm^3/g and microporous volume is 1.105 cm^3/g, indicating that it is mainly in the microporous range. The removal (%) of anionic dye MO increased from 30% to 100% by increasing the adsorbent dose from 0.01 to 0.08 g. Therefore, 0.05 g/L of adsorbent was chosen as the optimum dosage. The contact time for MO onto PAAC to reach equilibrium was 45 min, where the dye uptake (q_e) increased from 351.33 to 437.86 mg/g by increasing the
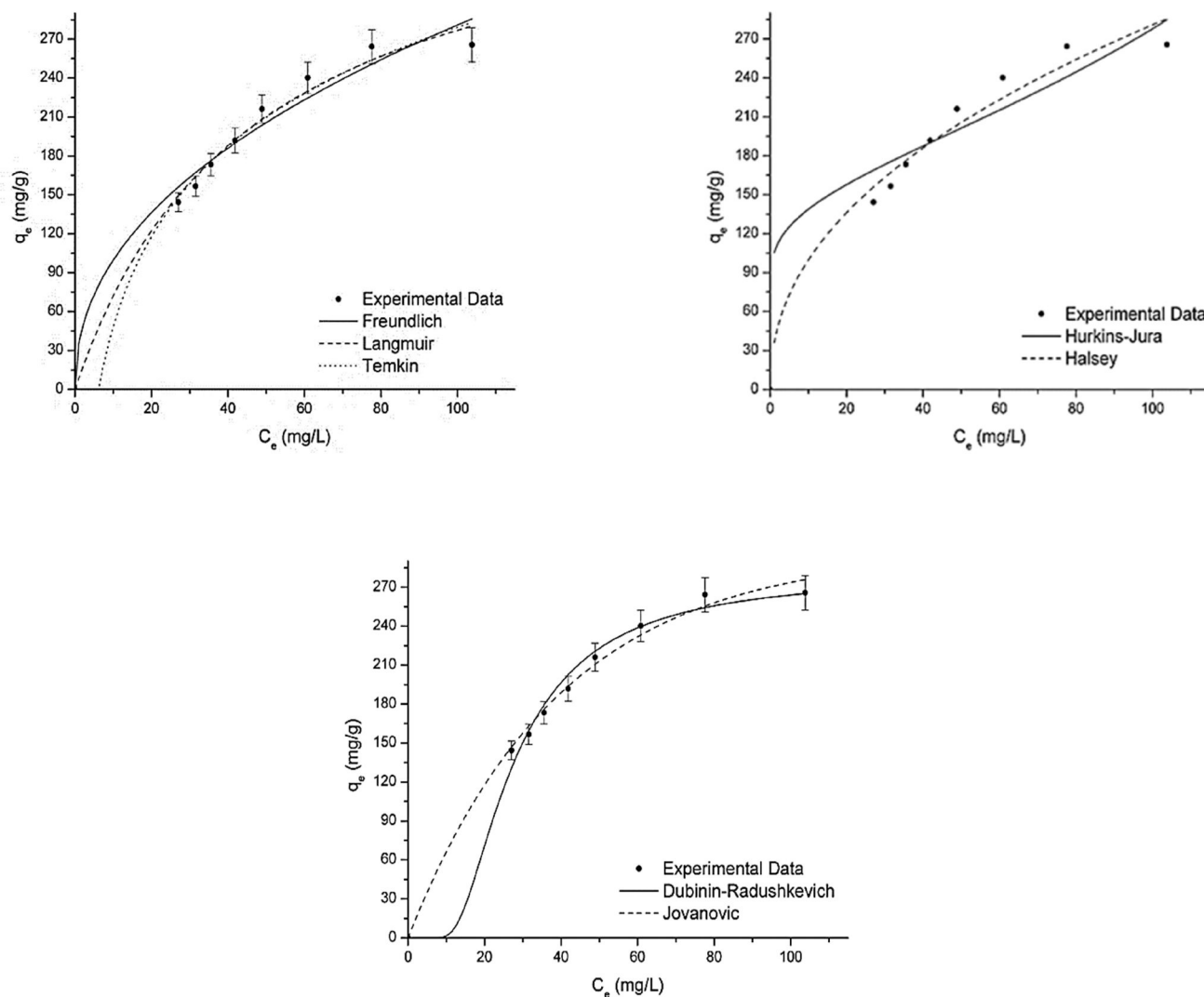
Figure 19. The adsorption isotherms of MO by GPAC (Samarghandi *et al.* 2009).

initial MO concentrations from 150 to 250 mg/L. A temperature increases from 283 to 323 K, led to a slight decrease in dye adsorption capacity from 257.54 to 245.56 mg/g. Several isotherm models (Langmuir, Freundlich, and Temkin) were evaluated, where the equilibrium uptake was best described by the Temkin isotherm. Several kinetic models (PFO, PSO, and Elovich) were used to fit the experimental data from the adsorption of MO onto PAAC, where the results showed that the kinetic data were in good agreement with the PSO kinetic model. The mechanism of adsorption was also investigated. The results of the intraparticle diffusion model suggested that it was not the only rate controlling step. The results indicate that PAAC could be employed as a low-cost alternative for the removal of MO from aqueous media.

The removal of MO by activated carbon (AC) derived from rice husk residue (RHR) wastes was studied by Li *et al.* (2016). RHR (30 g) was put into a flask with 200 mL of 3 M NaOH solution added into the reactor, where the temperature was increased to 105 °C and fixed for 5 h. The final AC product was washed and dried, then 2 g of base

treated solid residue (BTRHR) was treated with 15 mL H_3PO_4 aqueous solution at BTRHR/H_3PO_4 ratio of 1:2. The mixture was put into an oven at 100 °C for 24 h and then used for activation. Batch adsorption studies were conducted to examine the effects of contact time, pH (3–11), initial concentration (50–450 mg/L) and temperature (30–70 °C) on the removal of MO by AC-RHR. The surface was analyzed by FT-IR spectroscopy, TEM and the specific surface area and pore size of AC sample was tested by the BET method. The dye removal (%) gradually decreased from 63.8 to 57.9% with a pH increase from 3 to 9. The highest MO elimination was obtained at pH 3. The dye tended to increase as the temperature increased from 30 to 70 °C, indicating that adsorption of MO onto AC was endothermic in nature. The clearance rate of dye adsorbed decreased from 100 to 41.2% when the starting concentration increased from 50 to 250 mg/L. The MO dye system had an outstanding fit to the PSO kinetic model, according to the kinetic uptake profiles, which indicate that the MO adsorption rate is controlled by chemisorption. Desorption studies revealed that the adsorbed dye anions remained
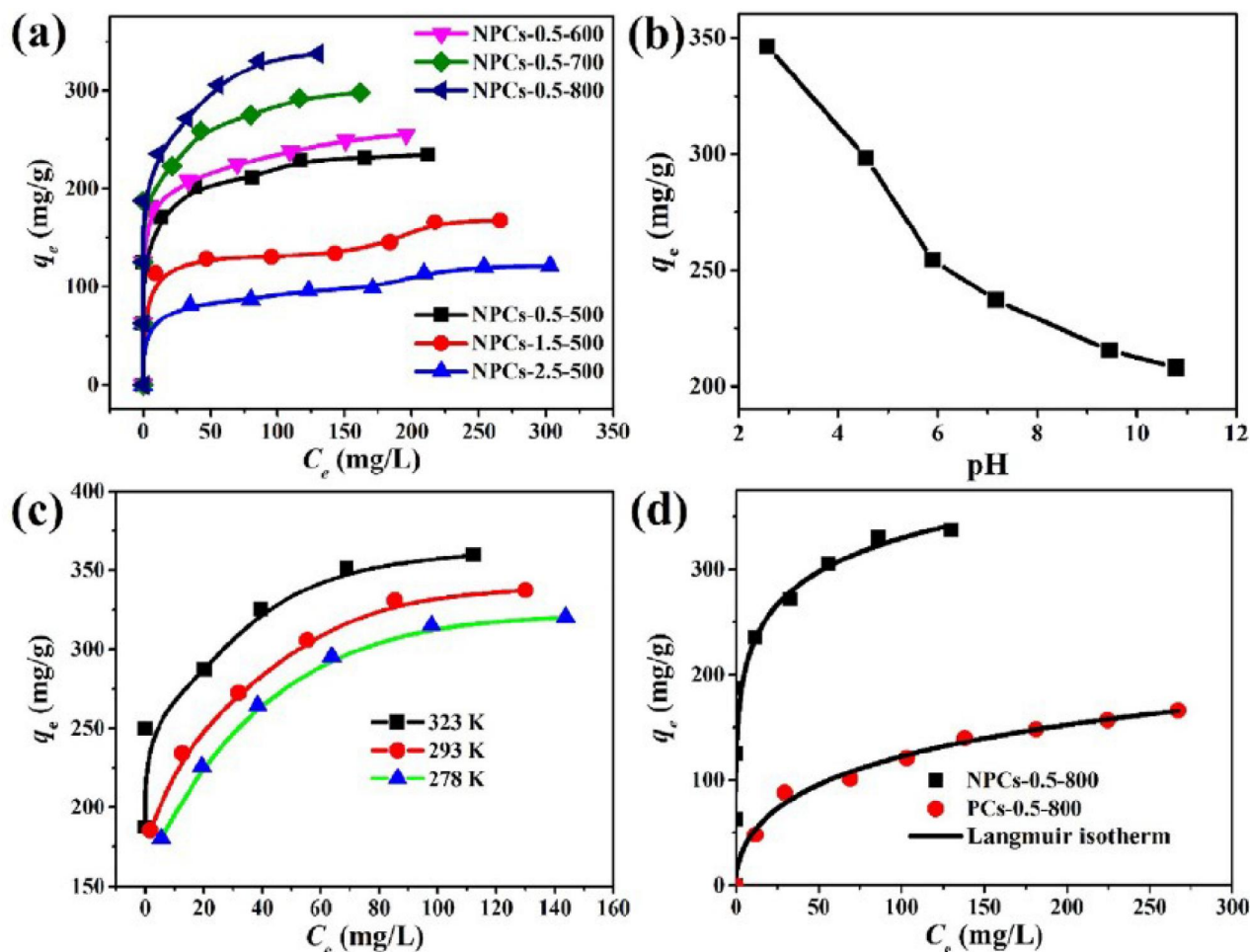
Figure 20. Adsorption isotherms of MO on samples (b) effect of pH on the adsorption capacity of MO on sample NPCs-0.5–800 (c) effect of temperature on the adsorption of MO on sample NPCs-0.5–800 (d) Langmuir isotherms for MO adsorption on NPCs-0.5–800 and PCs-0.5–800 (Sun *et al.* 2019).

almost stable on the adsorbent surface, which supports the role of chemisorption of MO onto the AC surface.

Waste cellulose fibers were employed by Sun *et al.* (2019) to create high-performance nitrogen-doped porous carbon adsorbents (NPCs), which were then used to remove MO from water. The NPCs were prepared *via* a spray drying process followed by thermal treatment. Different samples (0.5, 1.5 and 2.5 g of dried waste cellulose fibers was added to 40 mL of the zincoxen aqueous solution at room temperature. After being aged at −10 °C overnight, the mixture was thawed at room temperature and spray dried to obtain solid $Zn(EDA)_3^{2+}$/cellulose microspheres, which were subsequently calcined at various thermal temperatures (500, 600, 700 and 800 °C) in a N_2 atmosphere for 3 h. After washing with a 1.0 M nitric acid solution, followed by deionized water and ethanol, the solid product was then dried at 80 °C for 12 h to obtain a carbon sample. For example, NPCs-0.5–800 represents the carbon sample which was prepared with 0.5 g of cellulose fibers and thermally treated at 800 °C for 3 h. For comparison purpose, another carbon sample was prepared based on the procedure detailed above, but 0.5 g of cellulose power was used as carbon source and $ZnCl_2$ was used as the activating agent. The calcination temperature was 800 °C. This sample is denoted as PCs-0.5–800. The surface was characterized using XRD, field emission scanning

electron microscopy (FESEM), TEM and X-ray photoelectron spectroscopy (XPS). The specific surface areas were estimated by the BET method with the N_2 adsorption data in the relative pressure range of $P/P_0 = 0.005$–0.2. The influence of initial MO dye concentration, pH and temperature was investigated. The surface of the adsorbent was thermally treated at 800 °C with the highest specific surface area (1259.4 m^2/g) and total pore volume (2.7 cm^3/g) exhibited the best dye adsorption capacity (337.8 mg/g). In contrast, the (PCs-0.5–800) specific surface area of 1105.3 m^2/g, the volume (0.5 cm^3/g) and the adsorption capacity about 187.6 mg/g. The adsorption capacity of the MO dye on NPCs-0.5–800 declined (from 346 to 208 mg/g) as the pH increased from 2.6 to 10.8 as noted in Figure 20b. The optimum chosen pH was 7.1 and the adsorption capability of MO increased as the initial dye concentrations varied from 50 to 400 mg/L (cf. Figure 20a). The uptake of dye increased as the temperature rose from 278 to 323 K in Figure 20c, which demonstrates that MO adheres to NPCs *via* an endothermic process. The isotherm data is obeyed for both Langmuir and Freundlich isotherm models, but the Langmuir model yielded superior results for NPCs derived at lower temperature (278 K) due to a better correlation coefficient (0.998) as noted in Figure 20d. A maximum adsorption capacity of 337.8 mg·g^{-1} was obtained for

Table 8. Adsorption performance of MO by Group D adsorbents.

Adsorbent name	q_{max} (mg/g)	pH	Temp. (°C)	Model for q_{max} determination	Reference
AC from coconut shell fibers	75.58	4	50	Freundlich	(Singh et al. 2003)
AC from granular pine cone	404.40	7.5 ± 0.2	20.3	Langmuir	(Samarghandi et al. 2009)
AC from Phragmites australis	3.39×10^3	4	25	Temkin	(Chen S et al. 2010)
AC from rice husk	–	3	70	–	(Li et al. 2016)
AC from cellulose fibers by thermal treatment	337.80	2.6	20	Langmuir	(Sun et al. 2019)
AC from cellulose power with $ZnCl_2$	187.6	2,6	20	Langmuir	(Sun et al. 2019)
AC from endemic Vitis vinifera L. grape seeds	79.7	2	45	Freundlich	(Yönten et al. 2020)

Table 9. Kinetic parameters of pseudo-first order (PFO), pseudo-second order (PSO) models and thermodynamic parameters for adsorption of MO dye by Group D adsorbents.

Adsorbent name	k_1 (min^{-1})	k_2 (g/mg min)	Temp. (°C)	$\Delta H°$ (kJ mol^{-1})	$\Delta G°$ (kJ mol^{-1})	$\Delta S°$ (J mol^{-1} K^{-1})	Reference
AC from coconut shell fibers	–	–	25	82.15	34.24	0.16	(Singh et al. 2003)
AC from granular pine cone	0.01	0.0001	20 ± 0.2	–	–	–	(Samarghandi et al. 2009)
AC from Phragmites australis	7.02×10^{-2}	1.60×10^{-5}	22 ± 2	–	–	–	(Chen S et al. 2010)
AC from rice husk	–	–	–	–	–	–	(Li et al. 2016)
AC from cellulose fibers by thermal treatment	–	–	–	–	–	–	(Sun et al. 2019)
AC from cellulose power with $ZnCl_2$	–	–	–	–	–	–	(Sun et al. 2019)
AC from endemic Vitis vinifera L. grape seeds	–	–	15	24.80	−1.72	83.00	(Yönten et al. 2020)

adsorption of MO onto the surface of NPCs-0.5–800, according to the Langmuir isotherm model. The adsorption isotherm of dye on PCs-0.5–800 was also measured under the same conditions, which reveals that the adsorption capacity of PCs-0.5–800 was less than half for NPCs-0.5–800. The PFO and PSO kinetic adsorption models were used to measure the uptake profiles of MO dye onto the NPCs adsorbents. Based on the correlation coefficient values (R^2), the rate of adsorption was in good agreement with the PSO model.

The ability of AC derived from endemic Vitis vinifera L. grape seeds (AC-VVL) grown in the Tunceli-Elaz region to absorb MO was investigated by Yönten et al. (2020). For the preparation of sample, the seeds were cleaned of impurities and were left for 40 min at 120 °C in a muffle furnace. After 1 h, the temperature of the furnace was raised to 500 °C, and calcination was applied to the seeds. Batch adsorption experiments were achieved as a function of pH (2, 5, 8 and 11), temperature (15 °C, 30 °C and 45 °C) and initial concentration (100, 150, 300 and 1000 mg L^{-1}). The characterization of dye adsorption was analyzed pre-adsorption (AC-VVL) and post-adsorption (AC-VVL + dye) using FTIR, SEM and a BET analyzer. The Langmuir, Freundlich, Temkin and Harkins Jura isotherms were examined to describe the equilibrium profiles at variable temperature. At pH 2, the elimination effectiveness is at its highest, but it decreases until pH 11. The initial concentration value at equilibrium boosts the elimination effectiveness of MO on AC-VVL (55 min). The amount of MO adsorbed increases as the temperature rises. At 45 °C, the highest dye adsorption was obtained, which is well described by the Freundlich isotherm comparison to other isotherms (Langmuir, Temkin, and Harkins Jura isotherms) for all temperatures studied, with a maximum adsorption capacity of 79.7 mg/g. Thermodynamic parameters $\Delta G°$, $\Delta H°$ and $\Delta S°$ were calculated and the adsorption was endothermic ($\Delta H°$, positive), increased randomness of the adsorbent-dye system ($\Delta S°$, positive) and spontaneous process ($\Delta G°$, negative). In Table 8, the various AC and modified forms were used to remove MO from water and wastewater, which are ranked according to their adsorption capacities. Table 9 lists kinetic parameters of PFO, PSO models and thermodynamic parameters for adsorption of MO dye onto AC.

Group E: Composites

Composite adsorbents are a distinct category of adsorbents that consist of two or more component materials. The characteristics of the individual adsorbent components are usually distinct from the properties of the composite material formed by their resulting combination. Composite materials usually have better adsorption properties than the individual substance that comprise the composite (Iwuozor et al. 2021).

Chaukura et al. (2017) used biochar (BC) and Fe_2O_3–biochar nano-composites (Fe_2O_3-BC) which were prepared from $FeCl_3$-modified pulp and paper sludge (PPS) by pyrolysis at 750 °C as an effective adsorbent for the treatment of wastewater containing MO azo dye. BC was prepared by pyrolysis of dried PPS at 750 °C for 2 h. Fe_2O_3-BC was synthesized by pyrolysis of $FeCl_3$-modified PPS (1:3, m/v) at 750 °C for 2 h in a one-step pyrolysis method. The adsorbent surfaces were characterized by XRD, SEM and FTIR spectroscopy. The BET surface area (SBET), pore volume and pore size were calculated using an automated N_2 adsorption analyzer. Despite the lower BET surface area and porosity of Fe_2O_3-BC, its MO removal efficiency was 52.79%, which is higher than that for BC. The effect of experimental parameters such as contact time, pH, initial MO concentration, adsorbent dosage and temperatures were tested. BC showed a higher adsorption capacity at pH 2, while Fe_2O_3-BC had greatest adsorption capacity at pH 12. The adsorbent weight from 2.5 up to 12.5 g/L was accompanied by an increase in the removal efficiency of dye. Both BC and Fe_2O_3-BC
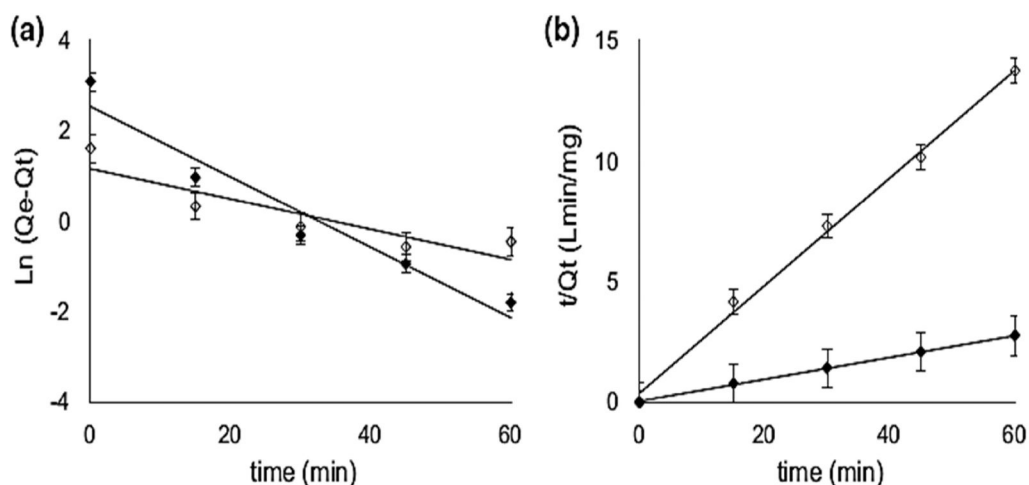
Figure 21. First and second order adsorption kinetics for MO adsorption on BC (open diamond) and Fe$_2$O$_3$-BC (filled diamond). error bars indicate standard error of the mean (Chaukura *et al.* 2017).

achieved 100% removal of azo dye at an adsorbent dosage of 5 g/L. The initial concentrations of the dye increased from 50 to 250 mg/L, the adsorption ability of the BC and Fe$_2$O$_3$-BC increased. The adsorption capacity of both adsorbents increased upon greater contact time, where 30 min was selected as the optimum time for both BC and Fe$_2$O$_3$-BC. Studies of the adsorption isotherms reported that, the equilibrium adsorption data were described by the Freundlich model. Kinetic data suggest that the adsorption kinetics for BC and Fe$_2$O$_3$-BC were best represented by the PSO model with R^2 values of 0.996 and 0.999, respectively (cf. Figure 21). The standard difference in the Gibbs energy ($\Delta G°$) for the adsorption process was -5.932 kJ mol^{-1} for BC and -7.344 kJ mol^{-1} for Fe$_2$O$_3$–BC, which supports the feasibility of these adsorbents for MO dye adsorption. More recently, Steiger *et al.* (2021) carried out an experimental and computational study on the adsorption of a series of ternary biopolymer-metal composites with a series of inorganic anions and dye adsorbate systems. Among the various dyes, the adsorption properties of the ternary biopolymer composite containing Al(III) was studied for its adsorption properties with methyl orange at variable concentration, where the Al(III) counterion was varied (chloride, nitrate, and sulfate). The key results for MO uptake relate to the tunable uptake according to the nature of the counterion in the ternary bio-composites, where the MO adsorption capacity is listed in descending order, as follows: nitrate > chloride > sulfate, in accordance with trends in hydration based on the Hofmeister series. The variation in MO uptake can be related to the lability of the counterion, in agreement with an ion exchange mechanism, where the nitrate counterion yields the highest adsorption capacity (ca. 300 mg/g) for the ternary bio-composite system (cf. Figure 5B) in Steiger *et al.* (2021). The synthetic strategy reported by Steiger *et al.* offers a facile, low cost and green synthetic method to design bio-adsorbents with tunable anion selectivity by judicious selection of the Al (III) salt precursors for controlled MO uptake in complex mixtures.

By using the co-precipitation method, (Blaisi *et al.* 2018) created date palm ash (DPA) and Mg-Al-layered double hydroxide (LDH) composites and characterized them using FTIR spectroscopy, SEM, XRD, and Brunauer-Emmett-Teller (BET). Using MO as a model for an acidic dye, the DPA-Mg-Al-LDH (DPA/Mg-Al) composites were employed to remove MO from the aqueous phase. Firstly, a known amount of magnesium and aluminum salts (M^{2+}: M^{3+}; 3:1 ratio) were dissolved in 50 mL of deionized water in a reactor equipped with a magnetic stirrer. A ratio of (0.5:2, 1:2 and 1.5:2) of DPA (g) and MgAl (g) corresponding to the MgAl- LDH was also sonicated for 1 h in 100 mL deionized water and transferred to the reaction vessel. The mixture was stirred for 15 min and pH 10 ± 0.5 at 90 °C. Then, the reaction was subjected to refluxing at 90 °C for 24 h, centrifuged, washed with deionized water and dried at 40 °C in an oven for 48 h for further use. Addition of date palm ash into the surface of Mg-Al-LDH increased the accessible surface area from 44.46 to 140.65 m^2/g, which results in improved adsorption. A rapid decrease in dye removal (%) was observed from pH 3 to 4, where no significant change in the removal was observed with a further increase in pH. The removal of MO on DPA/Mg-Al was achieved at an optimum pH 2. The maximum removal of 88% was observed for MO after 90 min by DPA/MgAl-2. The dye removal (%) for MO decreased from 88.68 to 12.16% with the addition of NaCl. The adsorbent reached a maximum adsorption capacity for a dye concentration of 84 mg/L, where no further dye was adsorbed onto the DPA/MgAl-2 surface at higher concentration. A maximum adsorption capacity (215 mg/g) was observed for DPA/MgAl-2 with MO. With an increase in adsorbent weight from 2 to 10 mg, the acidic dye removal efficiency increased. The correlation coefficient of the PSO kinetic model ($R^2 > 0.99$) was significantly higher than the PFO model, indicating that the adsorption of MO onto DPA/MgAl-2 were best-fit by PSO model. For the temperatures (298– 318 K), the Langmuir isotherm ($R^2 > 0.978$) model represented the adsorption system versus other models such as the Tempkin, Freundlich and Dubinin–Radushkevich (D-R) isotherms. The adsorbent surface displayed homogeneous features, where the maximum

adsorption capacity by DPA/MgAl-2 for MO was 243.0 mg/g at 298K. The thermodynamic adsorption parameters ($\Delta G°$, $\Delta H°$ and $\Delta S°$) for MO onto DPA/MgAl-2 were determined at 298, 308, and 318 K. The negative magnitudes of the parameters revealed that adsorption of MO on DPA/Mg-Al was spontaneous, exothermic and had reduced disorder after the adsorption process for the MO-DPA/MgAl system.

Haqiqi and Hikmawati (2019) used chicken eggshell and rice husk waste as a low-cost adsorbent of anionic MO. Chicken eggshells were washed with tap water and dried in the sun. After that, the chicken eggshell powder was heated at 105 °C for 15 min. Meanwhile, rice husk was washed with tap water, then dried, and heated at 105 °C for 15 min. Chicken eggshell powder and coarse rice husk were mixed and varied its composition ratio by 3:1, 2:1, 1:1, 1:2, and 1:3. The adsorption process of 50 mL MO (20 ppm) in aqueous solution with (11 g) of adsorbent was tested using the UV-Vis spectrophotometer at a fixed wavelength (465 nm). The chicken eggshell adsorbent combined with rice husk of the ratio of 1: 1 were able to adsorb MO from solution up to 27.70%. Thus, the ratio of chicken eggshell and rice husk influence the MO adsorption capacity, especially their significant size difference between chicken eggshell and rice husk.

Yusmaniar et al. (2020) created mesoporous silica composites with AC as an adsorbent using leftover rice husk and coconut shell as raw materials. Rice husk ash was hybridized with PEG into silica-PEG, and then PEG was released by solvothermal extraction using DMG (dimethyl sulfoxide) as solvent to obtain mesoporous silica. Composites were formed by homogenizing mesoporous silica and AC with methanol at 200 °C for 2h. Composites were successfully characterized by FTIR spectroscopy and SEM-EDX. The optimum pH for the adsorption of MO with the following adsorbents (mesoporous silica, activated carbon and mesoporous-activated carbon silica composites) was pH 2, where the maximum adsorption capacity (0.161, 0.415 and 0.398 mg/g) was estimated, respectively. Mesoporous silica, AC, and composites that effectively remove MO have respective weights of 0.4 g, 0.2 g, and 0.2 g and adsorption capacities of 0.115 mg/g, 0.235 mg/g, and 0.247 mg/g. The optimum contact time of mesoporous silica, activated carbon and mesoporous-AC silica composites with MO dye was selected at 30 min with maximum adsorption capacity of 0.119, 0.468 and 0.470 mg/g, respectively. Based on a regression value (R^2) of 0.9722, the Langmuir isotherm model favorably represented the adsorption process over the Freundlich isotherm. The adsorption kinetics show the third-order adsorption kinetics with a regression value (R^2) of 0.9989. The various composites used to remove MO from water and wastewater are given in Table 10 along with their adsorption capacities. Kinetic parameters for the PFO and PSO models, along with the thermodynamic parameters of adsorption for MO dye onto various composites are listed in Table 11.

Mechanism of MO adsorption

In this section, we discuss the mechanism of MO adsorption firstly based on the nature of the adsorbate, then on the nature of the adsorbent material. Studying the chemical nature of the adsorbent and adsorbate can provide an improved understanding of the specific physico-chemical mechanisms that are involved in the adsorption process. MO is a polycyclic aromatic compound that can have electron donor-acceptor (EDA) interactions with adsorbents with some level of aromaticity. These physical interactions can be in the form of π - π (8–12 kJ/mol), cation – π (8–25 kJ/mol) and anion – π (20–50 kJ/mol). These are some of the favorable physical interactions for MO uptake.

Table 10. Adsorption performance of MO by Group E adsorbents.

Adsorbent name	q_{max} (mg/g)	pH	Temp. (°C)	Model for q_{max} determination	Reference
Fe$_2$O$_3$–biochar nano-composites	46.60	3	25	Freundlich	(Chaukura et al. 2017)
Date palm ash and Mg-Al-layered double hydroxide composites	242.98	2	25	Langmuir	(Blaisi et al. 2018)
Chicken eggshell powder and coarse rice husk composites	–	–	–	–	(Haqiqi and Hikmawati 2019)
AC with mesoporous silica composites	0.47	2	room temperature	Langmuir	(Yusmaniar et al. 2020)
Ternary chitosan-alginate-metal biocomposites	42–467	7	23	Langmuir	(Steiger and Wilson 2022)

Table 11. Kinetic parameters of pseudo-first order (PFO), pseudo-second order (PSO) models and thermodynamic parameters for adsorption of MO dye by Group E adsorbents.

Adsorbent Name	k_1 (min^{-1})	k_2 (g/mg min)	Temp. (°C)	$\Delta H°$ (kJ mol^{-1})	$\Delta G°$ (kJ mol^{-1})	$\Delta S°$ (J mol^{-1} K^{-1})	Reference
Fe$_2$O$_3$–biochar nano-composites	0.08	12,427.39	25	–	−7.34	–	(Chaukura et al. 2017)
Date palm ash and Mg-Al-layered double hydroxide composites	0.06	0.13	25	−42.63	−8.56	−114.87	(Blaisi et al. 2018)
Chicken eggshell powder and coarse rice husk composites	–	–	–	–	–	–	(Haqiqi and Hikmawati 2019)
AC with mesoporous silica composites	–	–	–	–	–	–	(Yusmaniar et al. 2020)

Adsorbents like biochar and activated carbons are strongly aromatic that can interact with MO. The dye is also able to interact with adsorbents by hydrogen bonds (4–40 kJ/mol) The dimethyl substituted nitrogen atom on one end and the sodium substituted Sulfur atom on the other end are good sites for weak interactions with hydrogen species on adsorbents (cf. chemical structure of MO in Figure 1) (Iwuozor et al. 2021). The type of adsorbent materials also influences the relative adsorption capacity with the MO dye system. Bio-sorbents generally have lower porosity and surface areas but are capable of adsorptive uptake because they possess many functional groups that can facilitate various physico-chemical interactions (Hevira et al. 2021). Bio-sorption consists of mainly four primary mechanisms which are chemisorption, physisorption, microprecipitation and oxidation/reduction (Veglio and Beolchini 1997). Due to the complexity of the process, multiple mechanisms may contribute simultaneously during the process. Chemisorption consists of ion exchange, chelation (or coordination) and complexation, while electrostatic interactions and van der Waals forces fall under the category of physisorption. Surface functional groups play a significant role in binding the adsorbate in chemisorption (Vijayaraghavan and Balasubramanian 2015). Ion exchange occurs via electrostatic interactions between negatively charged groups of the biomass and the cations in solution (Abdolal et al. 2014), which is a reversible process. Activated carbons and biochar possess higher surface areas and are more porous. The surface area ensures the greater availability of active sites and adsorption capacity for MO. Based on the dimensions of the pores, the intraparticle diffusion may be slow, resulting in a rate-limiting step (Ighalo et al. 2021). Clays and minerals are well-ordered crystalline inorganic minerals. The sheet-like (2D) layered nature of clays suggest it can be pillared and intercalated to preserve its adsorptive potential and prevent swelling in contact with water (Yadav et al. 2021). It also follows that such clays can adsorb MO by ion exchange. The most frequently used adsorbent group are the composite adsorbents. This may be due to its perceived high adsorption activity which is contributed by the individual adsorbents that make up the composite. As well, composite materials offer a relatively facile and modular approach to the design of adsorbents with tailored properties, according the relative composition and stability of the resulting products. The modularity of the adsorbent design in the case of chitosan-based materials was highlighted in recent work reported by Mohamed et al. (2020) for chitosan-agrowaste bio-composites, along with for chitosan-based adsorbents with variable metal-ion doping (Steiger and Wilson, 2020, 2022) and (Udoetok et al. 2020) to achieve tailored adsorption properties. The choice of nanoparticle components in composite adsorbents may relate to their flexibility in the ability to incorporate within matrices due to their small size. Even though the composite material formed has distinct properties from its precursor parent material, the parent materials also contribute to the excellent properties of the composite material through stabilization effects (Iwuozor et al. 2021).

Desorption studies

Desorption studies help to elucidate the nature of adsorption and recycling of the dye. If the adsorbed dye can be desorbed using neutral pH water, then the attachment of the dye onto the adsorbent will possess weak bonding. If sulfuric acid or alkaline water desorbs the dye then the adsorption will be through ion-exchange. If an organic acid, such as acetic acid can desorb the dye, then the dye has been held by the adsorbent via chemisorption. Desorption processes are usually carried out by mixing a suitable solvent with the dye-saturated substrate and shaken together for fixed time, until the dye extract on the solvent and then using filtration to separate the adsorbent. The dye–solvent mixture dried at high temperature to evaporate the solvent (Bharathi and Ramesh 2013).

The desorption of MO dye from modified montmorillonite (MMT) with a cationic CTAB surfactant (CTMAB-MMT), or an anionic surfactant, sodium stearate (10SSTA-MMT) and their mixture with montmorillonite (CTMAB/10SSTA-MMT) were studied by Chen D et al. (2011). The desorption efficiency for the three samples was 3.2%, 8.4% and 11.5%, respectively. Very low desorption of dye represents bonding that occurs via strong interactions.

To check economic feasibility of the adsorption process, (Hosseini et al. 2011) studied the desorption process. Chemical reagents such as 1 M NaOH, 1 M KNO_3 and 0.01 M CTAB were employed as eluents. The results showed maximum recovery of MO when 1 M NaOH solution was used as the eluent, whereas the maximum desorption (67.12%) of anionic MO dye occurs in alkaline NaOH solution, which indicates that the adsorption occurs via an ion-exchange process. Desorption of MO increased by increasing the initial MO concentration. The desorption capacities of MO from CCM increase from 12.13 to 56.8 mg/g with greater initial MO concentration from 50 to 500 mg/L.

The desorption of MO from CTAB modified wheat straw (MWS) was investigated by Su et al. (2014). The results indicated the use of heated water resulted in greater regeneration efficiency (83.28%), which is practical and feasible. Therefore, it may be concluded that the MWS is an efficient, environmentally friendly, and economically feasible alternative with a promising agriculture absorbent for dye adsorption from industrial wastewater.

For the adsorption process to be economic, the desorption process of methyl orange dye (MO) from acrylic acid grafted Ficus carica fiber was studied by Gupta V et al. (2013). The desorption tests on MO-loaded adsorbent using 0.1 N NaOH as the eluting agent, were observed for four cycles. It was observed that the level of adsorption (%) of MO onto the adsorbent was 44.74% at optimized conditions and the recovery for the first cycle was 39.24% with 0.1 N NaOH. The desorption of sorbate with alkali explained that the adsorption of MO onto the adsorbent is mainly controlled by strong binding forces such as ionic or covalent bonding.

Desorption experiments were carried out by Lafi and Hafiane, (2016) to find the optimum pH-desorption

conditions. The results show that the desorption efficiency for MO at the first desorption cycle from an MO-adsorbed commercial coffee waste (MCWs) was achieved with increasing pH of the desorbing agent. Low desorption efficiency of 8.15 and 7.80% for MO-adsorbed CTAB modified commercial coffee waste (CW-CTAB) and MO-adsorbed CPC modified commercial coffee waste (CW-CPC) occurred in neutral distilled water, whereas greater desorption was demonstrated at more alkaline pH.

The desorption of methyl orange (MO) from active carbon prepared from endemic Vitis vinifera L. grape seeds (AC-VVL) was studied by (Yönten *et al.* 2020). Desorption experiments were performed with ethanol, methanol and acetone. Ethanol was found to have maximum efficiency of 45% the maximum recycling yield (%) was 29% for AC-VVL by using methanol solution at 288 K. The recovery of AC-VVL with acetone was 20% at 318 K. Desorption results report that ethanol had greater recycling yield (%) than other solutions to recover AC-VVL.

To study the ability to reuse modified algal biomass of Nannochloropsis sp. with CTAB surfactant (AlgN-CTAB) where adsorption with MO was performed by Buhani *et al.* (2021). The results of the adsorption-desorption of MO by AlgN-CTAB with 4 repetition cycles resulted in greater removal of MO above 80%. The AlgN-CTAB adsorbent can be used repeatedly and is very effective in absorbing MO from water.

Challenges and future prospects

According to the literature that has been so far examined, there is a need for more in-depth research on dye removal techniques as well as advancements in the fabrication and utilization of natural materials as unconventional adsorbents (Crini *et al.* 2019). Many strategies have recently been studied in an effort to create more affordable and efficient adsorbents. Natural materials are readily available, and various researchers have suggested using them as low-cost adsorbents. These substances may be employed as sorbents to draw MO from water and wastewater solutions. These include improving sorption capacity through modification whilst gaining an improved understanding of the adsorption mechanisms through mechanistic modeling. To determine the interactions and the role of functional groups in the dye adsorption process, it is important to further investigate how the adsorbate and adsorbent system interact. The molecular structure/surface group (both the form and size) of the adsorbents, as well as their adsorptive capabilities, require critical and systematic studies. It should also be tested whether using these natural materials with actual industrial dye wastewater (complex mixtures) is feasible. The practical use of natural materials as adsorbents is constrained for another reason because the mixture of adsorbate and adsorbent is challenging to separate after adsorption. Research is now being conducted to examine novel, feasible, and updated techniques that can more efficiently remove dyes from water and wastewater while also effectively separating natural materials from the two. In a recent study of the removal of inorganic sulfate from simulated groundwater samples, Solgi *et al.* (2020, 2023) employed chitosan-based composites in a pelletized form for fixed bed columns to enable dynamic separations. These fixed-bed columns allow for improved recovery and adsorbent regeneration in the form of pelletized materials over conventional powdered adsorbents. Thus, the utilization of such fixed bed columns is anticipated to address a number of the technical challenges encountered with conventional powdered adsorbents for separations carried out under equilibrium or dynamic conditions (Solgi *et al.* 2023; Steiger *et al.* 2023). To identify better methods for regeneration, there is a need for considerable research because recycling and regeneration of natural materials are crucial processes. Therefore, it is anticipated that the continued interest in the removal of azo dyes such as MO by employing inexpensive adsorbents would serve to address such biosorbent technology needs in the near future.

Conclusion

This review article discussed the need to remove anionic dyes such as methyl orange from water and wastewater due to its widespread use and relative toxicity. For the removal of hazardous contaminants such as MO from water bodies, adsorption techniques based on natural and modified natural materials-based adsorbents offer a green alternative for long-term sustainable treatment of contaminated water. The utilization of natural and modified natural materials as adsorbents for the removal of pollutants is promising due to their abundant functional groups and synthetic versatility. The latter is highlighted in the case of lignocellulosic biocomposites that offer a range of options according to the modular design of adsorbents that can be tailored to a range of applications for controlled removal of metal-ions such as Pb(II) (Mohamed *et al.* 2022), anionic dyes (Mohamed *et al.* 2020), and cationic dyes (Steiger *et al.* 2023). Adsorption capacity and other factors were examined that include the solution pH, adsorbent dosage, initial pollutant concentration, and temperature. The kinetic and thermodynamic parameters that affect the sorption processes have been reviewed for several categories of materials: *Clays and Minerals; Biosorbents; Biochar; Activated carbon; and Composites.* Although significant progress has been made in the field of inexpensive sorbents, much more study is still required to accurately predict the adsorption properties of adsorbents for the removal of anionic dyes from water under various operating conditions. Studying the elimination of a wider range pollutant components and their mixtures (*e.g.,* industrial wastewater) will contribute to this go*al.* In order to prevent secondary pollution, eco-friendly chemicals can also be utilized for synthetic modification, as demonstrated in the case of lignocellulosic biocomposites described above. In order to remove solid wastes, it is also necessary to improve the regeneration and recycling of post-use and spent adsorbent materials.

ORCID

Dhafir T. A. AL-Heetimi http://orcid.org/0000-0003-3694-8234
Lee D. Wilson http://orcid.org/0000-0002-0688-3102

References

Abdolal A, Guo W, Ngo H, Chen S, Nguyen N, Tung K. 2014. Typical lignocellulosic wastes and by-products for biosorption process in water and wastewater treatment: a critical review. Bioresour Technol. 160:57–66. doi: 10.1016/j.biortech.2013.12.037.

Agbovi HK, Wilson LD. 2021. Adsorption processes in biopolymer systems: fundamentals to practical applications. In: Natural polymers-based green adsorbents for water treatment. Chapter 1; Elsevier. p. 1–53. doi: 10.1016/B978-0-12-820541-9.00011-9.

Ahmadi M, Niari M, Kakavandi B. 2017. Development of maghemite nanoparticles supported on cross-linked chitosan (γ-Fe$_2$O$_3$@CS) as a recoverable mesoporous magnetic composite for affective heavy metals removal. J Mol Liq. 248:184–196. doi: 10.1016/j.molliq.2017.10.014.

Al-Heetimi DT, Dawood AH, Khalaf QZ, Himdan TA. 2012. Removal of methyl orange from aqueous solution by Iraqi bentonite adsorbent. Ibn Al-Haitham J Pure Appl Sci. 25(1):1–13.

Al-Kazragi MA, Al-Heetimi DT, Al-Khazrajy OS. 2019. Xylenol orange removal from aqueous solution by natural bauxite (BXT) and BXT-HDTMA: kinetic, thermodynamic and isotherm modeling. DWT. 145:369–377. doi: 10.5004/dwt.2019.23609.

Al-Kazragi MA, Al-Heetimi DT. 2021. Pretreated fishbone as low cost-adsorbent for cationic dye adsorption from aqueous solutions: equilibrium, optimization, kinetic and thermodynamic study. J Phys: conf Ser. 1879(2)(:022073. 1-16. doi: 10.1088/1742-6596/1879/2/022073.

Al-Ma'amar AA. 2012. Sorption study of methyl orange on the Iraqi kaolinite clay. JNUS. 15(4):98–103. doi: 10.22401/JNUS.15.4.12.

Annadurai G, Juang RS, Lee DJ. 2002. Use of cellulose-based wastes for adsorption of dyes from aqueous solutions. J Hazard Mater. 92(3): 263–274. doi: 10.1016/S0304-3894(02)00017-1.

Ardejani FD, Badii K, Limaee NY, Shafaei SZ, Mirhabibi AR. 2008. Adsorption of direct red 80 dyes from aqueous solution on to almond shells: effect of pH, initial concentration and shell type. J Hazard Mater. 151(2–3):730–737. doi: 10.1016/j.jhazmat.2007.06.048.

Atmani F, Bensmaili A, Amrane A. 2010. Methyl orange removal from aqueous solutions by natural and treated skin almonds. Desalination Water Treat. 22(1–3):174–181. [Mismatch doi: 10.5004/dwt.2010.1425.

Bazrafshan E, Zarei AA, Nadi H, Zazouli MA. 2014. Adsorptive removal of methyl orange and reactive red 198 dyes by *Moringa perina* ash. Indian J Chem Technol. 21:105–113.

Bechtold T, Burtscher E, Turcanu A. 2001. Cathodic decolorisation of textile wastewater containing reactive dyes using multi-cathode electrolyser. J Chem Technol Biotechnol. 76(3):303–311. doi: 10.1002/jctb.383.

Belay K, Hayelom A. 2014. Removal of methyl orange from aqueous solutions using thermally treated egg shell (locally available and low cost biosorbent). Int J Sci Res Innov. 8(1):43–49. doi: 10.13140/RG.2.1.2403.1449.

Bellifa A, Makhlouf M, Boumila ZH. 2017. Comparative study of the adsorption of methyl orange by bentonite and activated carbon. Acta Phys Pol A. 132(3):466–468. doi: 10.12693/APhysPolA.132.466.

Bhatnagar A, Sillanpää M. 2010. Utilization of agro-industrial and municipal waste materials as potential adsorbents for water treatment – a review. Chem Eng J. 157(2–3):277–296. doi: 10.1016/j.cej.2010.01.007.

Bhattacharjee C, Dutta S, Saxena V. 2020. A review on biosorptive removal of dyes and heavy metals from wastewater using watermelon rind as biosorbent. Environ Adv. 2:100007. doi: 10.1016/j.envadv.2020.100007.

Bharathi K, Ramesh S. 2013. Removal of dyes using agricultural waste as low-cost adsorbents: a review. Appl Water Sci. 3(4):773–790. doi: 10.1007/s13201-013-0117-y.

Blaisi NI, Zubair, M, Ihsanullah, Ali S, Kazeem TS, Manzar MS, Al-Kutti W, Al Harthi MA. 2018. Date palm ash-MgAl-layered double hydroxide composite: sustainable adsorbent for effective removal of methyl orange and eriochrome black-T from aqueous phase. Environ Sci Pollut Res Int. 25(34):34319–34331. doi: 10.1007/s11356-018-3367-2.

Boki K, Imai T, Ohno S. 1991. Adsorption of methyl orange on starches. J Food Sci. 56(1):90–92. doi: 10.1111/j.1365-2621.1991.tb07982.x.

Buhani, Suharso, Miftahza, N, Permatasari, Desy, Sumadi. 2021. Improved adsorption capacity of *Nannochloropsis* sp. through modification with cetyltrimethylammonium bromide on the removal of methyl orange in solution. Adsorp Sci Technol. 2021:1–14. doi: 10.1155/2021/1641074.

Chaukura N, Murimba EC, Gwenzi W. 2017. Synthesis, characterisation and methyl orange adsorption capacity of ferric oxide–biochar nano-composites derived from pulp and paper sludge. Appl Water Sci. 7(5):2175–2186. doi: 10.1007/s13201-016-0392-5.

Chen D, Chen J, Luan X, Ji H, Xia Z. 2011. Characterization of anion-cationic surfactants modified montmorillonite and its application for the removal of methyl orange. Chem Eng J. 171(3):1150–1158. doi: 10.1016/j.cej.2011.05.013.

Chen S, Zhang J, Zhang C, Yue Q, Li Y, Li C. 2010. Equilibrium and kinetic studies of methyl orange and methyl violet adsorption on activated carbon derived from *Phragmites australis*. Desalination. 252(1–3):149–156. doi: 10.1016/j.desal.2009.10.010.

Chen ZX, Jin XY, Chen Z, Megharaj M, Naidu R. 2011. Removal of methyl orange from aqueous solution using bentonite-supported nanoscale zero-valent iron. J Colloid Interface Sci. 363(2):601–607. doi: 10.1016/j.jcis.2011.07.057.

Crini G, Lichtfouse E, Wilson LD, Morin-Crini N. 2019. Conventional and non-conventional adsorbents for wastewater treatment. Environ Chem Lett. 17(1):195–213. doi: 10.1007/s10311-018-0786-8.

Das S, Barman S, Thakur R. 2012. Removal of methyl orange and methylene blue dyes from aqueous solution using low-cost adsorbent zeolite synthesized from fly ash. J Environ Sci Eng. 54(4): 472–480.

Deligeer W, Gao Y, Asuha S. 2011. Adsorption of methyl orange on mesoporous ɤ-Fe$_2$O$_3$/SiO$_2$ nanocomposites. Appl Surf Sci. 257(8): 3524–3528. doi: 10.1016/j.apsusc.2010.11.067.

Deniz F. 2013. Adsorption properties of low-cost biomaterial derived from *Prunus amygdalus* L. for dye removal from water. ScientificWorldJournal. 2013:961671–961678. doi: 10.1155/2013/961671.

El Maguana Y, Elhadiri N, Benchanaa M, Chikri R. 2020. Adsorption thermodynamic and kinetic studies of methyl orange onto sugar scum powder as a low-cost inorganic adsorbent. J Chem. 2020:1–10. doi: 10.1155/2020/9165874.

Eljiedi AA, Kamari A. 2017. Removal of methyl orange and methylene blue dyes from aqueous solution using lala clam (*Orbicularia orbiculata*) shell. AIP Conf Proc. 1847(1):1–9. doi: 10.1063/1.4983899.

Fadhil OH, Eisa MY. 2019. Removal of Methyl orange from aqueous solutions by adsorption using corn leaves as adsorbent material. jcoeng. 25(4):55–69. doi: 10.31026/j.eng.2019.04.05.

Fajrwati FI, Yandini NI, Anugrahwati M, Setyawati A. 2020. Adsorption study of methylene blue and methyl orange using green shell (Perna Viridis). EKSAKTA: J Sci Data Anal. 1(1):92–97. doi: 10.20885/EKSAKTA.vol1.iss1.art14.

Fan L, Zhou Y, Yang W, Chen G, Yang F. 2008. Electrochemical degradation of aqueous solution of Amarnath azo dye on ACF under potentiostatic model. Dyes Pigm. 76(2):440–446. doi: 10.1016/j.dyepig.2006.09.013.

Fernandes JV, Rodrigues AM, Menezes RR, Neves GD. 2020. Adsorption of anionic dye on the acid-functionalized bentonite. Materials. 13(16):3600. doi: 10.3390/ma13163600.

Fumba G, Essomba JS, Tagne GM, Nsami JN, Bélibi PD, Mbadcam JK. 2014. Equilibrium and kinetic adsorption studies of methyl orange

from aqueous solutions using kaolinite, metakaolinite and activated geopolymer as low cost adsorbents. JAIR. 3(4):156–163.

Gupta V, Pathania D, Sharma S, Agarwal S, Singh P. 2013. Remediation and recovery of methyl orange from aqueous solution onto acrylic acid grafted *Ficus carica* fiber: isotherms, kinetics and thermodynamics. J Mol Liq. 177:325–334. doi: 10.1016/j.molliq.2012. 10.007.

Gupta R, Pandit C, Pandit S, Gupta P, Lahiri D, Agarwal D, Pandey S. 2022. Potential and future prospects of biochar-based materials and their applications in removal of organic contaminants from industrial wastewater. J Mater Cycles Waste Manag. 24(3):852–876. doi: 10.1007/s10163-022-01391-z.

Haddadian Z, Shavandi MA, Abidin ZZ, Fakhru'L-Razi AH, Ismail MH. 2013. Removal methyl orange from aqueous solutions using dragon fruit (*Hylocereus undatus*) foliage. Chem Sci Trans. 2(3): 900–910.

Hameed BH, Mahmoud DK, Ahmad AL. 2008. Sorption of basic dye from aqueous solution by Pomelo citrus grandis peel in a batch system. Colloids Surf A Physicochem Eng Asp. 316(1–3):78–84. doi: 10.1016/j.colsurfa.2007.08.033.

Hameed BH. 2009. Removal of cationic dye from aqueous solution using Jack fruit peel as non-conventional low-cost adsorbents. J Hazard Mater. 162(1):344–350. doi: 10.1016/j.jhazmat.2008.05.045.

Haqiqi ER, Hikmawati DI. 2019. Influence of chicken eggshell powder ratio with coarse rice husk on methyl orange removal from aqueous solution. CHEESA. 2(1):33–41. doi: 10.25273/cheesa.v2i1.4335.

Hevira L, Zilfa, Rahmayeni, Ighalo JO, Aziz H, Zein R. 2021. *Terminalia catappa* shell as low-cost biosorbent for the removal of methylene blue from aqueous solutions. J Ind Eng Chem. 97:188–199. doi: 10.1016/j.jiec.2021.01.028.

Hosseini S, Ali M, Rasool M, Cheah W, Choong T. 2011. Carbon coated monolith, a mesoporous material for the removal of methyl orange from aqueous phase: adsorption and desorption studies. J Chem Eng. 171(3):1124–1131. doi: 10.1016/j.cej.2011.05.010.

Ighalo J, Adeniyi A, Adelodun A. 2021. Recent advances on the adsorption of herbicides and pesticides from polluted waters: performance evaluation via physical attributes. J Ind Eng Chem. 93: 117–137. doi: 10.1016/j.jiec.2020.10.011.

Iwuozor K, Ighalo J, Emenike E, Ogunfowora L, Igwegbe C. 2021. Adsorption of methyl orange: a review on adsorbent performance. CRGSC. 4(100179):100179. doi: 10.1016/j.crgsc.2021.100179.

Jafari A, Kakavandi B, Kalantary R, Gharibi H, Asadi A, Azari A, Babaei A, Takdastan A. 2016. Application of mesoporous magnetic carbon composite for reactive dyes removal: process optimization using response surface methodology. Korean J Chem Eng. 33(10): 2878–2890. doi: 10.1007/s11814-016-0155-x.

Jalil AA, Triwahyono S, Adam SH, Rahim ND, Aziz MA, Hairom NH, Razali NA, Abidin MA, Mohamadiah MK. 2010. Adsorption of methyl orange from aqueous solution onto calcined Lapindo volcanic mud. J Hazard Mater. 181(1–3):755–762. doi: 10.1016/j.jhazmat.2010.05.078.

Jeong C, Kim J, Baik J, Pandey S, Koh D. 2022. Facile approach to the fabrication of highly selective CuCl-impregnated *q*-Al$_2$O$_3$ adsorbent for enhanced CO performance. Mater. 15(18):1–14. doi: 10.3390/ma15186356.

Kalantry RR, Jonidi Jafari A, Esrafili A, Kakavandi B, Gholizadeh A, Azari A. 2016. Optimization and evaluation of reactive dye adsorption on magnetic composite of activated carbon and iron oxide. Desalin Water Treat. 57(14):6411–6422. doi: 10.1080/19443994.2015. 1011705.

Kamaru AA, Sani NS, Malek NA. 2016. Raw and surfactant-modified pineapple leaf as adsorbent for removal of methylene blue and methyl orange from aqueous solution. Desalin Water Treat. 57(40): 18836–18850. doi: 10.1080/19443994.2015.1095122.

Kan T, Jiang X, Zhou L, Yang M, Duan M, Liu P, Jiang X. 2011. Removal of methyl orange from aqueous solutions using a bentonite modified with a new Gemini surfactant. Appl Clay Sci. 54(2):184–187. doi: 10.1016/j.clay.2011.07.009.

Karimulla SK, Ravindhranath K. 2014. Extraction of methyl orange dye from polluted waters using bio-sorbents derived from *Thespesia populnea* and *Pongamia pinnata* plants. Der Pharma Chem. 6(4): 333–344.

Kermani M, Izanloo H, Kalantary RR, Salehi Barzaki H, Kakavandi B. 2017. Study of the performances of low-cost adsorbents extracted from *Rosa damascena* in aqueous solutions decolorization. DWT. 80:357–369. [Mismatch doi: 10.5004/dwt.2017.21019.

Khapre M, Shekhawa A, Saravanan D, Pandey S, Jugade R. 2022. Mesoporous Fe–Al-doped cellulose for the efficient removal of reactive dyes. Mater Adv. 3(7):3278–3285. doi: 10.1039/d2ma00146.

Khapre M, Pandey S, Jugade RM. 2021. Glutaraldehyde-cross-linked chitosan–alginate composite for organic dyes removal from aqueous solutions. Int J Biol Macromol. 190:862–875. doi: 10.1016/j.ijbiomac. 2021.09.026.

Kourim A, Malouki MA, Ziouche A. 2021. Thermodynamic and kinetic behaviors of copper (II) and methyl orange (MO) adsorption on unmodified and modified kaolinite clay. In: Clay and clay minerals. Chapter 3;IntechOpen. p. 45–59.

Krika F, Benlahbib OE. 2015. Removal of methyl orange from aqueous solution via adsorption on cork as a natural and low-coast adsorbent: equilibrium, kinetic and thermodynamic study of removal process. Desalination Water Treat. 53(13):3711–3723. doi: 10.1080/19443994.2014.995136.

Lafi R, Hafiane A. 2016. Removal of methyl orange (MO) from aqueous solution using cationic surfactants modified coffee waste (MCWs). J Taiwan Inst Chem Eng. 58:424–433. doi: 10.1016/j.jtice. 2015.06.035.

Leodopoulos C, Doulia D, Gimouhopoulos K, Triantis TM. 2012. Single and simultaneous adsorption of methyl orange and humic acid onto bentonite. Appl Clay Sci. 70:84–90. doi: 10.1016/j.clay. 2012.08.005.

Li Y, Zhang X, Yang R, Li G, Hu C. 2016. Removal of dyes from aqueous solutions using activated carbon prepared from rice husk residue. Water Sci Technol. 73(5):1122–1128. doi: 10.2166/wst.2015.450.

Lu Y, Jiang B, Fang L, Ling F, Gao J, Wu F, Zhang X. 2016. High performance NiFe layered double hydroxide for methyl orange dye and Cr(VI) adsorption. Chemosphere. 152:415–422. doi: 10.1016/j.chemosphere.2016.03.015.

Mittal A, Malviya A, Kaur D, Mittal J, Kurup L. 2007. Studies on the adsorption kinetics and isotherms for the removal and recovery of Methyl Orange from wastewaters using waste materials. J Hazard Mater. 148(1–2):229–240. doi: 10.1016/j.jhazmat.2007.02.028.

Mohamed MH, Udoetok IA, Wilson LD. 2020. Animal biopolymer-plant biomass composites: synergism and improved sorption efficiency. J Compos Sci. 4(1):15. doi: 10.3390/jcs4010015.

Mohamed MH, Udoetok IA, Solgi M, Steiger BGK, Zhou Z, Wilson LD. 2022. Design of sustainable biomaterial composite adsorbents for point-of-use removal of lead ions from water. Front Water. 4: 739492. doi: 10.3389/frwa.2022.739492.

Ni ZM, Xia SJ, Wang LG, Xing FF, Pan GX. 2007. Treatment of methyl orange by calcined layered double hydroxides in aqueous solution: adsorption property and kinetic studies. J Colloid Interface Sci. 316(2):284–291. doi: 10.1016/j.jcis.2007.07.045.

Okoronkwo NE, Igwe JC, Uruakpa HN. 2008. Dye removal from waste water by adsorption onto boiler fly ash. Err Aquat Environ Toxicol. 2(1):44–48.

Okoro H, Pandey S, Ogunkunle C, Ngila C, Zvinowanda C, Jimoh I, Lawal I, Orosun M, Adeniyi A. 2022. Nanomaterial-based biosorbents: adsorbent for efficient removal of selected organic pollutants from industrial wastewater. Emerg Contam. 8:46–58. doi: 10.1016/j.emcon.2021.12.005.

Omidinasab M, Rahbar N, Ahmadi M, Kakavandi B, Ghanbari F, Kyzas G, Martinez S, Jaafarzadeh N. 2018. Removal of vanadium and palladium ions by adsorption onto magnetic chitosan nanoparticles. Environ Sci Pollut Res Int. 25(34):34262–34276. doi: 10.1007/s11356-018-3137-1.

Pandey S, Ramontja J. 2016. Guar gum-grafted poly(acrylonitrile)-templated silica xerogel: nanoengineered material for lead ion removal. J Anal Sci Technol. 7(1):1–15. doi: 10.1186/s40543-016-0103-8.

Pandey S, Son N, Kang M. 2022. Synergistic sorption performance of karaya gum crosslink poly (acrylamide-*co*-acrylonitrile) @ metal

nanoparticle for organic pollutants. Int J Biol Macromol. 210:300–314. doi: 10.1016/j.ijbiomac.2022.05.019.

Pandey S, Son N, Kim S, Balakrishnan D, Kang M. 2022. Locust Bean gum-based hydrogels embedded magnetic iron oxide nanoparticles nanocomposite: advanced materials for environmental and energy applications. Environ Res. 214(Pt 3):114000. doi: 10.1016/j.envres.2022.114000.

Papić S, Koprivanac N, Božić AL, Meteš A. 2004. Removal some reactive dyes from synthetic wastewater by combined Al(III) coagulation/carbon adsorption process. Dyes Pigm. 62(3):291–298. doi: 10.1016/S0143-7208(03)00148-7.

Potgieter JH, Pardesi C, Pearson S. 2021. A kinetic and thermodynamic investigation into the removal of methyl orange from wastewater utilizing fly ash in different process configurations. Environ Geochem Health. 43(7):2539–2550. doi: 10.1007/s10653-020-00567-6.

Purbaningtias TE, Wiyantoko B, Kurniawati P, Ruwindya Y. 2015. Removal of methyl orange in aqueous solution using rice husk. Proceeding in the 1st International Seminar on Chemical Education. Yakarta, Indonesia. 30:241–246.

Samarghandi MR, Hadi M, Moayedi S, Barjasteh FA. 2009. Two-parameters isotherms of methyl orange sorption by pinecone derived activated carbon. Iran J Environ Health Sci Eng. 6(4):285–294.

Sejie FP, Nadiye-Tabbiruka MS. 2016. Removal of methyl orange (MO) from water by adsorption onto modified local clay (kaolinite). Phys Chem. 6(2):39–48. doi: 10.5923/j.pc.20160602.02.

Shah SS, Sharma T, Dar BA, Bamezai RK. 2021. Adsorptive removal of methyl orange dye from aqueous solution using populous leaves: insights from kinetics, thermodynamics and computational studies. JECE. 3:172–181. doi: 10.1016/j.enceco.2021.05.002.

Singh KP, Mohan D, Sinha S, Tondon GS, Gosh D. 2003. Color removal from wastewater using low-cost activated carbon derived from agricultural waste material. Ind Eng Chem Res. 42(9):1965–1976. doi: 10.1021/ie020800d.

Sohrabi MR, Ghavami M. 2008. Photo catalytic degradation of Direct Red 23 dye using UV/TiO$_2$: effect of operational parameters. J Hazard Mater. 153(3):1235–1239. doi: 10.1016/j.jhazmat.2007.09.114.

Solgi M, Tabil LG, Wilson LD. 2020. Modified biopolymer adsorbents for column treatment of sulfate species in saline aquifers. Materials. 13(10):2408–2425. doi: 10.3390/ma13102408.

Solgi M, Steiger BGK, Wilson LD. 2023. A fixed-bed column with an agro-waste biomass composite for controlled separation of sulfate from aqueous media. Separations. 10(4):262–282. doi: 10.3390/separations10040262.

Steiger BGK, Wilson LD. 2020. Modular chitosan-based adsorbents for tunable uptake of sulfate from water. Int J Mol Sci. 21(19):7130–7146. doi: 10.3390/ijms21197130.

Steiger BGK, Udoetok IA, Faye O, Wilson LD. 2021. Counterion effects in metal hybrid biopolymer materials for sulfate adsorption: an experimental and computational study. ACS Appl Polym Mater. 3(9):4595–4606. doi: 10.1021/acsapm.1c00706.

Steiger BGK, Wilson LD. 2022. Ternary metal-alginate-chitosan composites for controlled uptake of methyl orange. Surfaces. 5(4):429–444. doi: 10.3390/surfaces5040031.

Steiger BGK, Zhou Z, Anisimov IA, Evitts RW, Wilson LD. 2023. Valorization of agro-waste biomass as composite adsorbents for sustainable wastewater treatment. Ind Crops Prod. 191:115913–115923. doi: 10.1016/j.indcrop.2022.115913.

Su Y, Jiao Y, Dou C, Han R. 2014. Biosorption of methyl orange from aqueous solutions using cationic surfactant-modified wheat straw in batch mode. Desalin Water Treat. 52(31–33):6145–6155. doi: 10.1080/19443994.2013.811121.

Subbaiah MV, Kim DS. 2016. Adsorption of methyl orange from aqueous solution by aminated pumpkin seed powder: kinetics, isotherms,

and thermodynamic studies. Ecotoxicol Environ Saf. 128:109–117. doi: 10.1016/j.ecoenv.2016.02.016.

Sultana M, Rownok M, Sabrin M, Rahaman M, Alam S. 2022. A review on experimental chemically modified activated carbon to enhance dye and heavy metals adsorption. Clean Eng Technol. 6:100382. doi: 10.1016/j.clet.2021.100382.

Sun B, Yuan Y, Li H, Li X, Zhang C, Guo F, Liu X, Wang K, Zhao XS. 2019. Waste-cellulose-derived porous carbon adsorbents for methyl orange removal. J Chem Eng. 371:55–63. doi: 10.1016/j.cej.2019.04.031.

Tang J, Yang ZF, Yi YJ. 2012. Enhanced adsorption of methyl orange by vermiculite modified by cetyltrimethylammonium bromide (CTMAB). Procedia Environ Sci. 13:2179–2187. doi: 10.1016/j.proenv.2012.01.207.

Tchuifon DR, Anagho SG, Njanja E, Ghogomu JN, Ndifor-Angwafor NG, Kamgaing T. 2014. Equilibrium and kinetic modelling of methyl orange adsorption from aqueous solution using rice husk and egussi peeling. Int J Chem Sci. 12(3):741–761.

Teng MY, Lin SH. 2006. Removal of methyl orange dye from water onto raw and acid activated montmorillonite in fixed beds. Desalination. 201(1–3):71–81. doi: 10.1016/j.desal.2006.03.521.

Tetteh S, Zugle R, Ofori A, Adotey JP. 2019. Kinetics and equilibrium thermodynamic studies of the adsorption of phenolphthalein and methyl orange onto muscovite clay. Front Chem. 2(1):33–37. doi: 10.22034/FCR.2020.122175.1017.

Udoetok IA, Faye O, Wilson LD. 2020. Adsorption of phosphate dianions by hybrid inorganic–biopolymer polyelectrolyte complexes: experimental and computational studies. ACS Appl Polym Mater. 2(2):899–910. doi: 10.1021/acsapm.9b01123.

Veglio F, Beolchini F. 1997. Removal of metals by biosorption: a review. Hydrometallurgy. 44(3):301–316. doi: 10.1016/S0304-386X(96)00059-X.

Vijayaraghavan K, Balasubramanian R. 2015. Is biosorption suitable for decontamination of metal-bearing wastewaters? A critical review on the state-of-the-art of biosorption processes and future directions. J Environ Manage. 160:283–296. doi: 10.1016/j.jenvman.2015.06.030.

Wang S, Boyjoo Y, Choueib A, Zhu ZH. 2005. Removal of dyes from aqueous solution using fly ash and red mud. Water Res. 39(1):129–138. doi: 10.1016/j.watres.2004.09.011.

Yadav S, Yadav A, Bagotia N, Sharma AK, Kumar S. 2021. Adsorptive potential of modified plant-based adsorbents for sequestration of dyes and heavy metals from wastewater - a review. J Water Process Eng. 42(102148):102148. doi: 10.1016/j.jwpe.2021.102148.

Yönten V, Sanyürek NK, Kivanç MR. 2020. A thermodynamic and kinetic approach to adsorption of methyl orange from aqueous solution using a low cost activated carbon prepared from *Vitis vinifera* L. Surf Interfaces. 20(100529):100529. doi: 10.1016/j.surfin.2020.100529.

Yu J, Zhang X, Wang D, Li P. 2018. Adsorption of methyl orange dye onto biochar adsorbent prepared from chicken manure. Water Sci Technol. 77(5–6):1303–1312. doi: 10.2166/wst.2018.003.

Yusmaniar Y, Erdawati E, Ghifari YF, Ubit DP. 2020. Synthesis of mesopore silica composite from rice husk with activated carbon from coconut shell as absorbent methyl orange color adsorbent. IOP Conf Ser: mater Sci Eng. 830(3)(:032078. doi: 10.1088/1757-899X/830/3/032078.

Zayed AM, Abdel Wahed MS, Mohamed EA, Sillanpää M. 2018. Insights on the role of organic matters of some Egyptian clays in methyl orange adsorption: isotherm and kinetic studies. Appl Clay Sci. 166:49–60. doi: 10.1016/j.clay.2018.09.013.

Zhou Y, Lu J, Zhou Y, Liu Y. 2019. Recent advances for dyes removal using novel adsorbents: a review. Environ Pollut. 252(Pt A):352–365. doi: 10.1016/j.envpol.2019.05.072.